Development of a Low-Frequency Piezo-ceramic Transducer Optimized for the Generation of a Plane Fundamental Shear Horizontal Guided Wave

by

Guillaume BOIVIN

THESIS PRESENTED TO ÉCOLE DE TECHNOLOGIE
SUPÉRIEURE IN PARTIAL FULFILLMENT OF THE REQUIREMENTS FOR
MASTER OF APPLIED SCIENCE IN MECHANICAL ENGINEERING
M.A.Sc.

MONTREAL, OCTOBER 24TH, 2016

ÉCOLE DE TECHNOLOGIE SUPÉRIEURE
UNIVERSITÉ DU QUÉBEC

BOARD OF EXAMINERS

THIS THESIS HAS BEEN EVALUATED

BY THE FOLLOWING BOARD OF EXAMINERS:

Prof. Pierre Bélanger, Memorandum Supervisor
Department of Mechanical Engineering at École de technologie supérieure

Prof. Martin Viens, Co-supervisor
Department of Mechanical Engineering at École de technologie supérieure

Prof. Ricardo J. Zednik, President of the Board of Examiners
Department of Mechanical Engineering at École de technologie supérieure

Prof. François Blanchard, External Examiner
Department of Electrical Engineering at École de technologie supérieure

THIS THESIS WAS PRESENTED AND DEFENDED

IN THE PRESENCE OF A BOARD OF EXAMINERS AND THE PUBLIC

ON SEPTEMBER 22^{ND}, 2016

AT ÉCOLE DE TECHNOLOGIE SUPÉRIEURE

ACKNOWLEDGEMENTS

I would like to thank, first, my advisor, Prof. Pierre Bélanger, and my co-advisor, Prof. Martin Viens, for their patience, their precious advice, and their significant support. Special thanks to Prof. Pierre Bélanger for his devotion and his full dedication to all of his projects and students. Throughout my entire Masters, he has been of great help and support, even during challenging times.

A special mention also to all my colleagues: Daniel Peirera, Alexandre Abid, David Lemonnier, Shreyank Gupta, Pierre Comot, Frédéric Dupont, and Christophe Travaglini. I enjoyed the valuable discussions and moments spent with all of you. Special thanks to Christophe, with who I shared a lot of significant time and who helped me solve my small everyday challenges.

This project was made possible thanks to the Consortium for Research and Innovation in Aerospace in Québec (CRIAQ) and especially to all the partners involved in the CRIAQ DPHM-501 project: École de technologie supérieure, Université de Sherbrooke, McGill University, Bombardier Aerospace, L3-MAS and the National Research Council. I would also like to thank Prof. Ricardo Zednik for his patience, precious advice, and knowledge; his support was invaluable to me.

Finally, this accomplishment would have never been possible, were it not for my beloved girlfriend Virginie, who has continuously been supporting me and smiling, even when I was not!

DÉVELOPEMENT D'UN TRANSDUCTEUR ULTRASONORE PIÉZOCÉRAMIQUE BASSE FRÉQUENCE POUR LA GÉNÉRATION D'ONDES GUIDÉES SUIVANT LE MODE DE CISAILLEMENT HORIZONTALE FONDAMENTAL

Guillaume BOIVIN

RÉSUMÉ

La surveillance de l'état des structures (SES) consiste à évaluer l'intégrité de structures de manière continue à l'aide de systèmes intégrés. Les inspections ultrasonores sont une des méthodes fréquemment utilisées afin de réaliser une telle tâche. Cette méthode a considérablement évolué grâce au domaine du contrôle non destructif (CND) par l'utilisation des ondes de volume, dans un premier temps, et ensuite par celle des ondes guidées. Un important défi émanant de l'utilisation des ondes ultrasonores en SES est la minimisation de l'impact des transducteurs utilisés sur les structures interrogées. Un second défi de taille, que ce soit en SES ou en CND, est le traitement de signal complexe requis par la nature multimodale et dispersive des ondes guidées. Une solution simple et massivement adoptée pour contrer cette dernière difficulté est l'utilisation de fréquences se situant sous la première fréquence de coupure, évitant ainsi les modes d'ordre supérieur. Une solution complémentaire consiste en l'utilisation du mode de cisaillement horizontal fondamental (SH_0), le seul mode d'onde ultrasonore guidée n'étant pas dispersif dans une plaque mince.

Ce mémoire de maîtrise s'intéresse au développement d'une méthode de conception d'un transducteur ultrasonore piézo-céramique optimisé pour la génération de l'onde SH_0 et la minimisation des modes de Lamb fondamentaux (A_0 et S_0). La première étape de la méthodologie proposée consiste à sélectionner le matériau ainsi que le mode vibratoire les plus appropriés; incidemment, le PZT-5H et le cisaillement dans l'épaisseur. La seconde étape consiste en l'optimisation de deux paramètres géométriques : la longueur et la largeur de l'élément actif rectangulaire. Ceux-ci ont une incidence directe sur l'amplitude des trois modes fondamentaux générés ainsi que sur l'ouverture et le nombre de lobes de directivités de ceux-ci. La géométrie a donc été déterminée conjointement avec la fréquence centrale désirée du transducteur afin de satisfaire au mieux les deux critères de performance préalablement établis. Quatre combinaisons, jugées ainsi satisfaisantes, ont été déterminées et leur comportement a été validé, dans un premier temps, grâce à une simulation analytique de propagation d'onde cylindrique. Un modèle analytique a initialement été utilisé puisqu'une modélisation par élément fini en trois dimensions, nécessaire pour ce type d'application, requiert une puissance de calcul significative. Ces résultats ont par la suite été validés par simulation par éléments finis en trois dimensions sur le logiciel commercial Abaqus. La combinaison des paramètres finaux: longueur de 25.4 mm, largeur de 3.7 mm et fréquence centrale de 425 kHz, ont, en dernier lieu, été expérimentalement validés au moyen d'un vibromètre laser 3D. À la lumière des résultats, il s'avère possible de générer une onde SH_0 dont l'amplitude est supérieure d'au moins 16.4 dB par rapport à celle des modes fondamentaux de Lamb dans toutes les directions. Cette sélectivité grimpe à 23.0 dB sur une ouverture de 20 degrés autour de la direction de propagation de l'onde SH_0.

Mots clés: Ondes Guidées, Surveillance de l'État des Structures, Mode Fondamental de Cisaillement Horizontale, Piézo-céramique, Transducteur

DEVELOPMENT OF A LOW-FREQUENCY PIEZO-CERAMIC TRANSDUCER OPTIMIZED FOR THE GENERATION OF A PLANE FUNDAMENTAL SHEAR HORIZONTAL GUIDED WAVE

Guillaume BOIVIN

ABSTRACT

Structural health monitoring (SHM) consists of continuously assessing structural integrity using integrated testing systems. One well-known method to achieve such a goal is ultrasonic testing. This technique has considerably evolved through non-destructive testing (NDT) by the use of, initially bulk ultrasonic waves and, subsequently, guided ultrasonic waves. One of the main challenges that emerges from the use of ultrasonic testing for SHM applications is to minimize the overall footprint of the specifically designed transducers. Another important challenge, either for NDT or SHM applications, is the requirement for complex signal processing due to the multimodal and dispersive nature of the guided waves. One simple and extensively used method to avoid the former case is to use frequencies under the first cut-off frequency to avoid high-order modes. A second complementary method to avoid the latter case is to use the fundamental shear horizontal (SH) guided wave mode (SH_0), which is the only non-dispersive guided wave mode propagating in a thin plate.

This masters thesis focuses on the development of a method to design a piezo-ceramic ultrasonic transducer optimized for the generation of the SH_0 mode and the minimization of both fundamental Lamb modes (A_0 and S_0). The proposed methodology consists of first choosing the proper piezoelectric material based on the best suited vibrational mode, which is PZT-5H in thickness-shear mode respectively. The second step is to optimize two geometrical parameters, the width and the length of the rectangular active element. Both parameters have a direct influence on the relative amplitude of the three generated modes as well as the aperture and the number of generated mode directivity lobes. Based on these criteria, four combinations have proven to be of sufficient interest, and their behaviour was validated using an analytical wave-propagation simulation. Such modeling was used because the required three-dimensional (3D) finite-element (FE) simulations are very computationally intensive when it comes to wave propagation. The results and analytical model accuracy were then validated using Abaqus finite-element software. The final optimal geometry and frequency combination, 25.4 mm long, 3.7 mm wide, and 1 mm thick, centered at 425 kHz, was finally experimentally validated using a laser Doppler vibrometer system to obtain the resulting complete 3D wave field. The results show that it is possible to generate a plane SH_0 wave at a relative amplitude of at least 16.4 dB above both fundamental Lamb modes in any direction, and of 23.0 dB within an aperture of 20 degrees.

Keywords: Guided Waves, Structural Health Monitoring, Shear Horizontal Fundamental Mode, Piezo-ceramic, Transducer

TABLE OF CONTENTS

LIST OF TABLES

Page

LIST OF FIGURES

LIST OF ABREVIATIONS

1D	One-dimensional
3D	Three-dimensional
ALID	Absorbing Layer with Increasing Damping
ECT	Eddy-current testing
EMAT	Electromagnetic acoustic transducer
FE	Finite-element
FEM	Finite-element modeling
FFT	Fast Fourier transform
GW	Guided wave
LDV	Laser Doppler vibrometer
LPI	Liquid penetrant inspection
NDE	Non-destructive evaluation
NDT	Non-destructive testing
PMNT	Lead magnesium niobate titanate
PVDF	Polyvinylidene fluoride
PZT	Lead zirconate titanate
SH	Shear horizontal
SHM	Structural Health Monitoring
SV	Shear vertical
UT	Ultrasonic testing

LISTE OF SYMBOLS AND UNITS OF MEASUREMENTS

$^\circ$	Degree
θ	Angle
$\frac{\partial}{\partial}$	Partial derivative
∇^2	3D Laplace operator
ρ	Density
λ	First Lamé coefficient
μ	Second Lamé coefficient
ϕ	Scalar potential function
Φ	Vector potential function
π	Pi
ν	Poisson's ratio
ε_{ij}^{T}	Dielectric coefficient tensor under constant stress
d_{ij}	Piezoelectric coefficient matrix
d_{ijk}	Piezoelectric coefficient tensor
d_{ijk}^{T}	Piezoelectric coefficient tensor under constant stress
s_{ijkl}^{E}	Compliance tensor under constant electric field
A	Wave complex amplitude
A_i	Lamb antisymmetric mode of order i
S_i	Lamb symmetric mode of order i

SH_i	Shear horizontal mode of order i
b	Half thickness of the plate
cos	Cosine function
C	Coulomb
dB	Decibel
c	Speed of sound
c_L	Longitudinal wave velocity
c_S	Shear wave velocity
c_g	Group velocity
c_p	Phase velocity
D_i	Dielectric displacement matrix
e	Napier's constant
E	Young's modulus
E_i	Electric field component in the *i* direction
E_m	Excitability of the m^{th} mode
f	Frequency in Hz
g	Gram
$H_0^{(1)}$	Zeroth order Hankel function of the first kind
Hz	Hertz
k	Wavenumber

k_L	Longitudinal wave wavenumber
k_S	Shear wave wavenumber
k_i	Wavenumber in the i direction
k_{SH}	Shear horizontal wave wavenumber
L	Transducer length
m	Meter
N	Newton
Pa	Pascal
$\vec{r}$	Position vector
sin	Sine function
S_{ij}	State of strain matrix
t	Time
t	Transducer thickness
tan	Tangent function
T_{jk}	State of stress matrix
$\vec{u}$	Displacement vector
$\vec{u_L}$	Zero curl displacement field
$\vec{u_T}$	Zero divergence displacement field
c_{ij}	Elasticity matrix coefficient
w	Transducer width
ω	Angular frequency

INTRODUCTION

Non-destructive testing (NDT) of materials and structures is a relatively recent field of study and research. In fact, it has drastically evolved since its first known appearance at the end of the nineteenth century. In addition, NDT involves many techniques: from simple visual inspections and liquid penetrant inspection (LPI) to more advanced techniques like eddy-current testing (ECT), acoustic emission, and ultrasonic testing (Cartz (1995)). All these different techniques are based on different physical phenomena but have a common goal, either to ensure the tested structural integrity or to characterize the properties of the tested material.

NDT techniques have turned out to be of even greater interest toward the end of the last century, not only for their value in assessing structural integrity, but also for their cost reduction ability. In fact, industries like nuclear, oil and gas, aerospace, and civil engineering have demonstrated increasing interest over the years in the improvement of traditional NDT techniques and the development of new methods to improve the reliability of installations and reduce the frequency of inspection, hence reducing operating and maintenance costs. Structural health monitoring (SHM) has more recently emerged as an even better cost-reducing solution. This field is interested in continuously assessing the integrity of structures without the periodicity aspect of inspections necessitated by NDT by integrating sensing systems or devices into the structures (Balageas *et al.* (2006)). This way, structures are constantly monitored, and maintenance or replacement of parts can be carried out only when required. Systems do not have to be constantly stopped to be systematically inspected, hence resulting in considerable savings.

Since every NDT technique is based upon different physical phenomena, every one of them requires different knowledge and experience. For this reason, and since the focus of this masters thesis is on ultrasonic testing, only this technique will be discussed in detail.

Ultrasonic testing started as bulk ultrasonic testing (conventional ultrasounds) allowing the detection of flaws in the volume of thick structures with the use of relatively high frequencies

(over 1 MHz). More recently, ultrasonic guided wave testing has been developed, allowing the fast screening or scanning of large thin structures and even inaccessible or fluid loaded structures (Leinov *et al.* (2015)). Unlike bulk ultrasonic waves, ultrasonic guided waves are dispersive, meaning that their velocity (phase and group) change with respect to the frequency, leading to much more difficulty in the use of such waves (Cheeke (2012)). Moreover, when increasing the frequency-thickness product, an infinity of guided wave modes will propagate in a media, further complicating the use of guided waves.

It appears that one plate-guided wave mode, the fundamental shear horizontal (SH) mode (SH_0), is not dispersive. This precise characteristic has led to the use and the development of many methods using the SH_0 wave (Fortunko *et al.* (1982), Ratassepp *et al.* (2008) and Demma *et al.* (2003)). Unfortunately, SH waves are more complicated to generate and to receive, due to their particular particle motion compared to the other classes of plate-guided waves. Few techniques have been used in the past to achieve the transduction of SH waves, such as using electromagnetic acoustic transducers (EMAT) or piezoelectric transducers (piezoelectric ceramics and piezoelectric polymers). Historically, EMAT was the chosen method due to the ease of generation (Hiroa and Ogi (1999)). Unfortunately, such methods are not suited for SHM applications due to their low transduction efficiency, and their important weight, which has led researchers to start using piezoelectric materials (Zhou *et al.* (2015)), as they have been frequently used for bulk wave and Lamb wave generation. To this day, no study has been conducted in order to develop a low-frequency piezoceramic transducer optimized for the generation of the SH_0 mode.

The objective of this masters thesis is therefore to develop a piezoceramic acoustic transducer optimized for the generation of the SH_0 wave at a high level of selectivity compared to the fundamental Lamb modes (A_0 and S_0) applications. Moreover, the optimization methodology

could easily be reused for slightly different applications, such as an ultrasonic transducer suited for NDT applications or for the generation of different ultrasonic modes.

In the first chapter of this masters thesis, the required theoretical background is reviewed so that fundamental knowledge to achieve the aim of this work is well understood. The first chapter also presents a brief review of the literature concerning SH-wave transduction. The second chapter is a paper that was submitted for publication in the journal *Ultrasonics* in July 2016. This paper discusses the methodology of the development of the transducer, the simulations that were carried out, and the experimental validation of the designed transducer. Finally, Chapter 3 is the conclusion in which the aim of this masters thesis, as well as all the completed work, is reviewed. In this section, the conclusions on the efficiency of the proposed method are drawn, and the possibilities for future work are discussed.

CHAPTER 1

THEORETICAL BACKGROUND AND LITERATURE REVIEW

In order to properly develop a transducer optimized for the generation of the SH_0 mode and for the reduction of other undesired modes, it is crucial to first understand the fundamentals of the three topics involved in such a device: ultrasound, piezoelectricity, and mechanical vibration. This chapter discusses the essential theoretical background of these three topics. Second, a review of the state of the art of the generation of guided waves is presented.

1.1 Ultrasound Fundamentals

Ultrasonic waves have been studied since the middle of the eighteenth century by many renowned scientists. Many excellent textbooks discuss the topic in detail as well as the historical evolution of ultrasound (Rose (1999), Cheeke (2012) and Graff (1991)). For this reason, only the essential theoretical elements are discussed in this section.

An ultrasonic wave can propagate in gas, liquid, and solid media at frequencies above 20 kHz. In the latter case, an ultrasonic wave is, by definition, a propagating mechanical stress wave (Cheeke (2012)). Many different types of ultrasonic waves exist: bulk waves (commonly called conventional ultrasound), surface waves (Rayleigh waves), plate-guided waves (including Lamb and SH waves), and many others.

1.1.1 Wave Propagation in Solid Bulk Media

To understand the nature of ultrasonic guided waves, one has to first understand bulk waves, often referred to as conventional ultrasound. Bulk waves that propagate in an infinite solid media are mechanical stress waves that depend on space and time. Their propagation properties depend on the elasticity, density, and homogeneity of the medium. These statements will be discussed below.

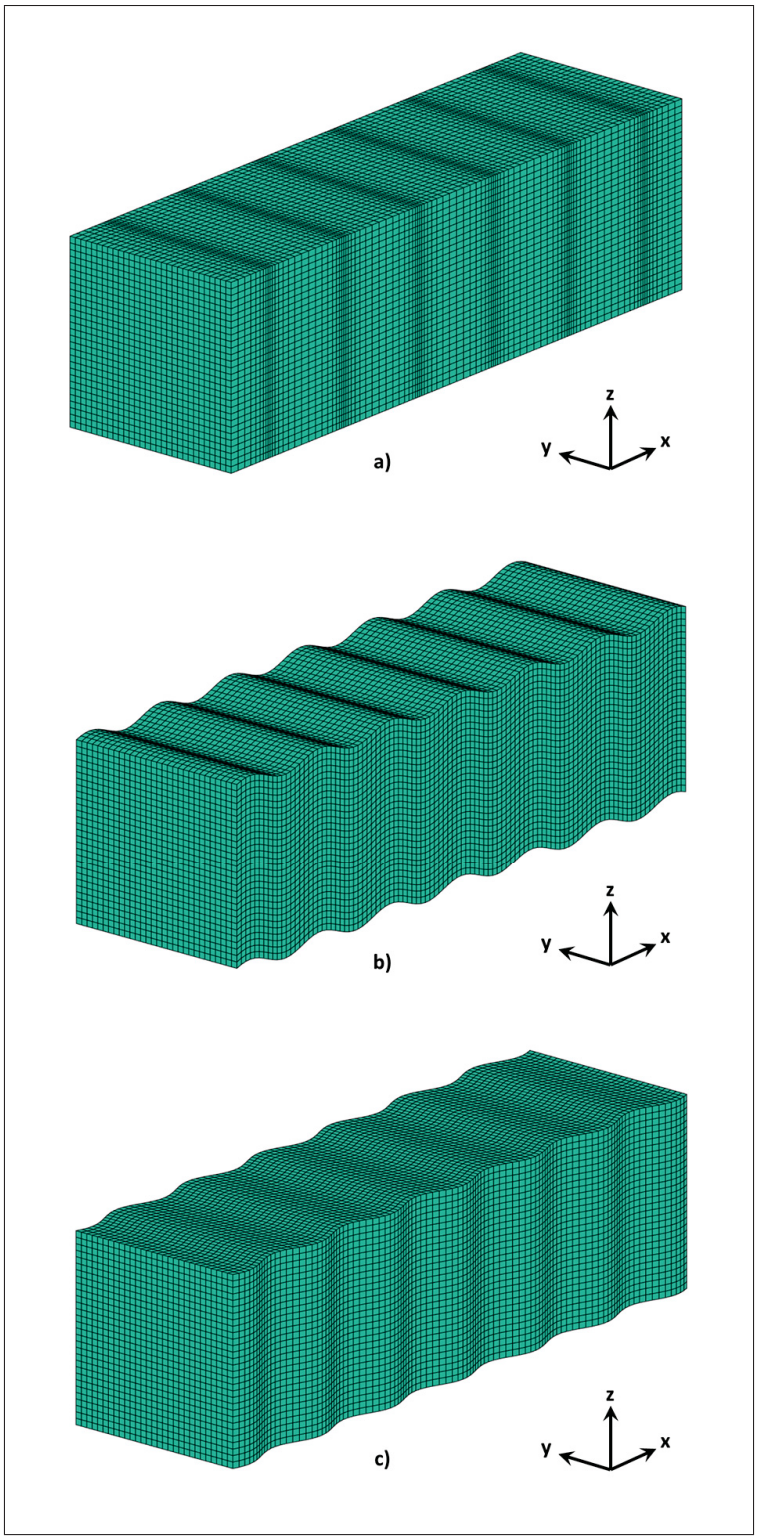

Figure 1.1 Deformation related to the propagation of bulk waves in the x direction in an isotropic homogeneous solid: a) longitudinal wave (P-wave or L-wave), b) shear vertically polarized wave (SV wave), and c) shear horizontally polarized wave (SH wave)

Bulk waves are the result of perturbation in an unbounded media or semi-infinite media. Figure 1.1 illustrates the three bulk waves that can propagate in solids. Two types of particle motion lead to these three different bulk waves propagating in the x direction, according to Figure 1.1. Motion in the x direction is the longitudinal wave (often referred to as the P-wave or pressure wave), while the motion normal to the propagation direction, in Figure 1.1 in the y and z directions, results in two distinct shear waves: one shear-vertical wave (SV wave, z direction) and one SH wave (y direction). All other types of ultrasonic wave modes come from the interaction of these three fundamental bulk ultrasonic modes with discontinuities, such as boundaries, interfaces, or even defects. Ultrasonic waves are described, similar to electromagnetic waves, by the wave equation. The one-dimensional wave equation was first discovered by d'Alembert and was detailed in three dimensions shortly after by Euler in the mid-eighteenth century (Cheeke (2012)). The 1D wave equation is

$$\frac{\partial^2 u}{\partial t^2} = c^2 \frac{\partial^2 u}{\partial x^2}, \tag{1.1}$$

where u is the 1D particle displacement, c is the speed of sound in the propagating media, x represents the position, and t is the time.

By definition, if a plane wave is propagating in a given direction $\vec{n} = \vec{e}_x n_x + \vec{e}_y n_y + \vec{e}_z n_z$, its 3D displacement can be written as

$$\vec{u}(\vec{r},t) \equiv A \cdot f(\vec{n} \cdot \vec{r} - c \cdot t), \tag{1.2}$$

where A is the initial wave amplitude, $\vec{r}$ is the position vector, t is the time, and f is an arbitrary function of space and time. If time and space are inseparable in the f function, this means that the wave is propagating. On the other hand, if space and time are independent in the f function, the result is a standing wave. The minus-sign stands for a wave that propagates in the positive x direction according to the reference coordinate system of Figure 1.1.

The 3D equation of motion or wave equation in the case of an isotropic homogeneous elastic medium can be expressed in terms of displacement using Navier's equation without any body

forces (Lamb (1917)):

$$\frac{\partial^2 \vec{u}}{\partial t^2} = (\lambda + \mu)\vec{\nabla}(\vec{\nabla} \cdot \vec{u}) + \mu \nabla^2 \vec{u}, \tag{1.3}$$

where ρ is the density of the medium, and λ and μ are its Lamé constants, which are related to the elasticity tensor of the material by $c_{11} = \lambda + 2\mu$ and $c_{44} = \mu$. This equation comes from the combination of Newton's second law with Hooke's law of elasticity. Rewriting equation 1.3 in terms of elasticity, we obtain

$$\frac{\partial^2 \vec{u}}{\partial t^2} = (c_{11} - c_{44})\vec{\nabla}(\vec{\nabla} \cdot \vec{u}) + c_{44} \nabla^2 \vec{u}, \tag{1.4}$$

Using the Helmholtz decomposition theorem, one can rewrite the displacement field vector as a sum of the gradient of a scalar potential, ϕ, and the curl of a vector potential, Φ (Cheeke (2012)):

$$\vec{u} = \vec{\nabla}\phi + \vec{\nabla} \times \Phi = \vec{u_L} + \vec{u_T}, \tag{1.5}$$

where $\vec{u}_L$ is a zero curl displacement field and $\vec{u}_T$ is a zero divergence displacement field. Substituting equation 1.5 into equation 1.4 leads to two independent separable equations, one representing the pure longitudinal motion (P-wave) depending only on ϕ,

$$\frac{\partial^2 \phi}{\partial t^2} = c_L^2 \nabla^2 \phi, \tag{1.6}$$

and one depending only on Φ, representing a pure shear motion:

$$\frac{\partial^2 \Phi}{\partial t^2} = c_S^2 \nabla^2 \Phi, \tag{1.7}$$

where c_L and c_S are respectively the longitudinal wave velocity and shear-wave velocity in such a medium. These velocities can be expressed as

$$c_L = \sqrt{\frac{c_{11}}{\rho}} = \sqrt{\frac{\lambda + 2\mu}{\rho}} \tag{1.8}$$

$$c_S = \sqrt{\frac{c_{44}}{\rho}} = \sqrt{\frac{\mu}{\rho}}. \tag{1.9}$$

This demonstration proves that, as stated before, only two types of waves can propagate in an unbounded medium. In the case of a harmonic monochromatic wave, the general solution of equations 1.6 and 1.7 is

$$\phi, \Phi = A \cdot e^{i(\omega \cdot t - k_{L,S} \cdot x)}, \tag{1.10}$$

where A is an unknown, ω is the angular frequency, t is the time, x is wave propagation direction, and $k_{L,S}$ are the wavenumbers of the longitudinal and shear wave, which can be written as

$$k_{L,S} = \frac{\omega}{c_{L,S}} \tag{1.11}$$

1.1.2 Plate-Guided Waves

When bulk waves are being propagated in bounded media, the interaction of these waves with the boundaries can lead to the generation and propagation of other types of waves. Plate-guided waves are non-vanishing waves that result from the propagation of bulk waves in a traction-free surface plate of finite thickness. Two different techniques were developed in the past in order to obtain the plate-guided-wave equations. The first one is based on the partial waves reflections (Cheeke (2012)) and the second one is a potential based technique (Lamb (1917)).

1.1.2.1 Shear Horizontal Waves

Shear horizontal waves represent the simplest case of plate-guided waves. In fact, as shown in Figure 1.2, these waves propagate due to the continuous reflections of the horizontally polarized shear bulk waves (SH waves) on the traction-free surfaces of the plate, where the guided-wave is propagating in the positive x direction. In fact, it is the simplest case because the wave is polarized along a single axis (z) and because SH modes are decoupled from partial waves propagating in the sagittal plane (xy plane according to Figure 1.2): the SV wave and the pressure wave.

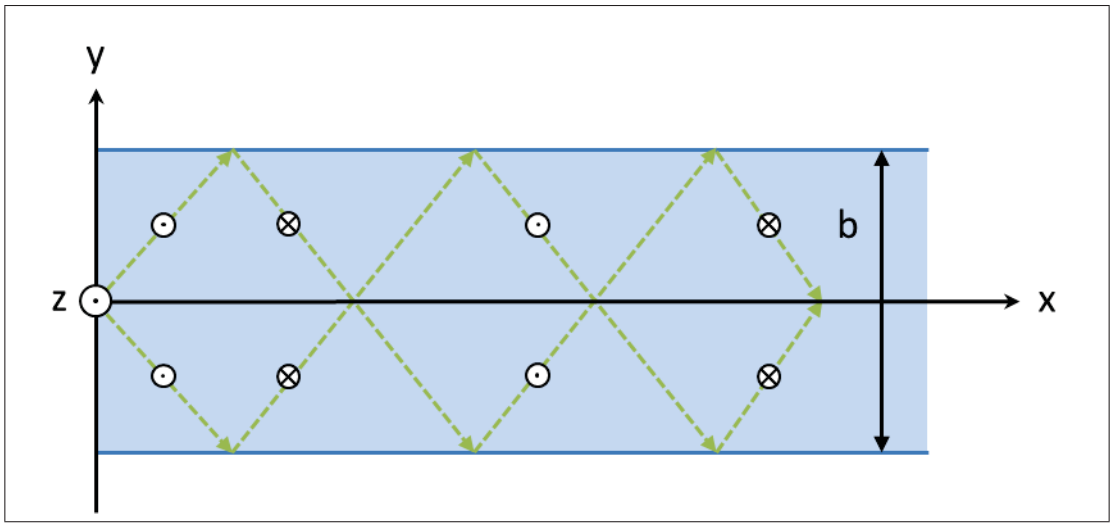

Figure 1.2 Shear horizontally polarized bulk wave (SH wave): multiple reflections on the surfaces of a plate leading to the propagation of shear-horizontal plate-guided waves

The simplest way to obtain the SH wave equation is to use the partial wave method as stated by Cheeke (2012). This method starts with the simple decomposition of the total wave field as the sum of three wavenumbers related to the three coordinate system axes, as

$$k^2 = k_x^2 + k_y^2 + k_z^2 = \frac{\omega^2}{c_S^2}. \tag{1.12}$$

Since the resulting wave is propagating in the x direction, k_x represents the propagating guided SH wavenumber, while the total wavenumber represents the incident bulk SH polarized wave. The wavenumber k_z is equal to zero, since no total or partial wave is propagating in the z direction. Finally, k_y represents the portion of the wave propagating in the thickness direction of the plate. It can be expressed using the boundary conditions at the surfaces of the plate, leading to solutions that correspond to transverse resonance for which k_y must be equal to $\frac{n\pi}{b}$, where b is the thickness of the plate and n is an integer. The wavenumber of the SH guided wave can be rewritten as:

$$k_x^2 = \left(\frac{\omega}{c_S}\right)^2 - \left(\frac{n\pi}{b}\right)^2 = k_{SH}^2. \tag{1.13}$$

Moreover, by definition, the propagating wavenumber can be written as $k_{SH}^2 = (\omega/c_p)^2$, which leads to the phase velocity equation:

$$c_p(fb) = \pm c_S \left(\frac{2fb}{\sqrt{4(fb)^2 - n^2 c_S^2}} \right), \tag{1.14}$$

where f is the frequency. It clearly appears from equation 1.14 that for $n = 0$, which represents the fundamental SH wave (SH_0), the phase velocity is equal to the shear bulk velocity for any value of frequency-thickness product. This explains why SH_0 is the only plate-guided-wave mode that is not dispersive, as every other possible modes has a changing phase velocity with increasing frequency-thickness product. In the case of non-zero values of n representing high-order SH modes, the denominator in equation 1.14 has to be real in order for the mode to propagates. This phenomenon is called the cut-off frequency product. The first frequency-thickness product allowing a real solution of the square root of the denominator of equation 1.14 is the cut-off product of the n^{th} mode, given by

$$(fb)_n = \frac{n c_S}{2}. \tag{1.15}$$

Below this precise frequency-thickness product, a mode is called evanescent or vanishing, meaning that no energy of this mode is propagating. Figure 1.3 illustrates the phase velocity dispersion curves of the SH waves in a 1.588 mm thick aluminum plate ($E = 70.8$ GPa, $\nu = 0.34$, and $\rho = 2700$ kg/m^3). These curves were computed using the DISPERSE software package (Pavlakovic *et al.* (1997)). Another important aspect of dispersive guided waves to understand and thus to define is the group velocity. The group velocity, for dispersive waves, represents the velocity at which the energy of a wave packet is traveling; it can be observed as the velocity of the maximum of the envelope of a dispersive wave packet. The group velocity inverse is mathematically obtained by differentiating the wavenumber equation 1.13, with respect to

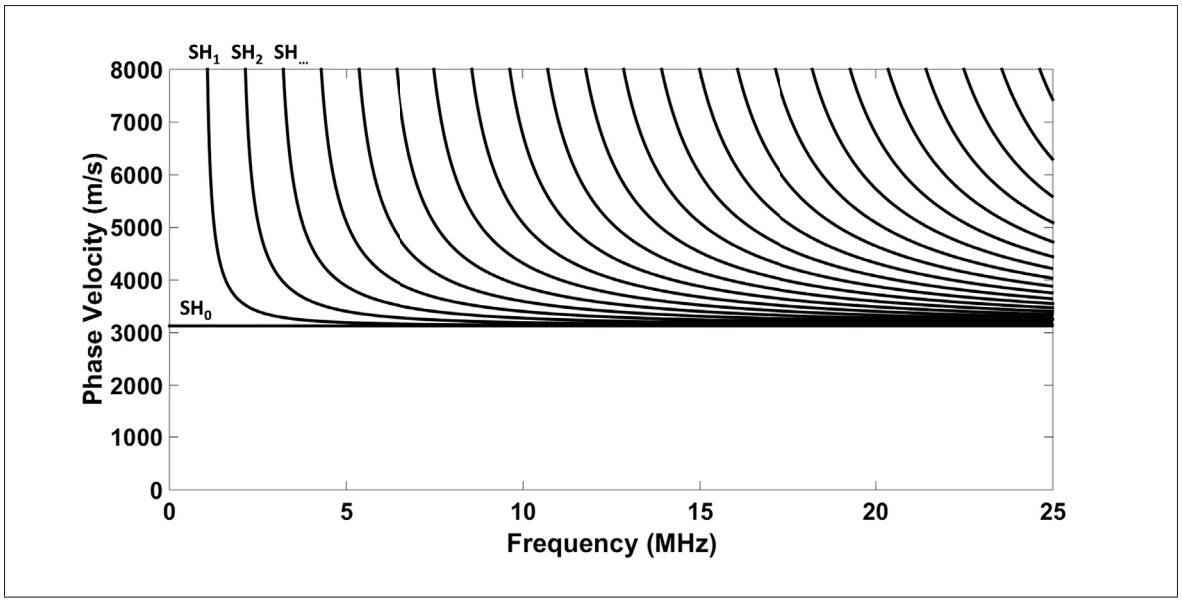

Figure 1.3 Phase velocity dispersion curves of the SH waves in a 1.588 mm aluminum plate (E = 70.8 GPa, ν = 0.34, and ρ = 2700 kg/m^3), curves computed using DISPERSE software packages (Pavlakovic *et al.* (1997))

frequency, which, after simplification and rearrangement, is

$$c_g(fb) = c_s \sqrt{1 - \frac{(n/2)^2}{(fb/c_S)^2}}. \tag{1.16}$$

Figure 1.4 represents the group velocity dispersion curves for the same medium as Figure 1.3, obtained with the same software.

1.1.2.2 Lamb Waves

Lamb waves are a more complex solution of the same free-plate problem. In fact, these types of waves are more mathematically complicated because they originate from the coupled interaction of both waves in the sagittal plane: the partial pressure wave and the partial vertically polarized shear wave at the traction-free surfaces of the plate. The two conditions for Lamb waves to propagate are that these two partial waves cannot be uncoupled and that they both have to satisfy the traction-free boundary condition of the surfaces. Another important aspect

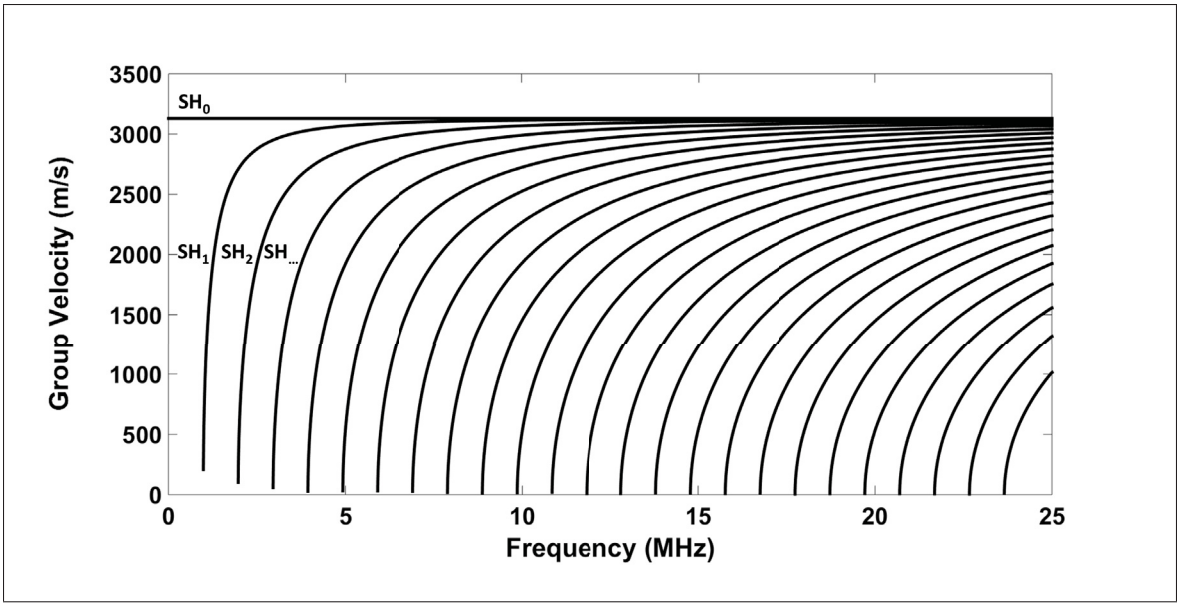

Figure 1.4 Group velocity dispersion curves of the SH waves in a 1.588 mm aluminum plate (E = 70.8 GPa, ν = 0.34, and ρ = 2700 kg/m^3), curves computed using DISPERSE software packages (Pavlakovic *et al.* (1997))

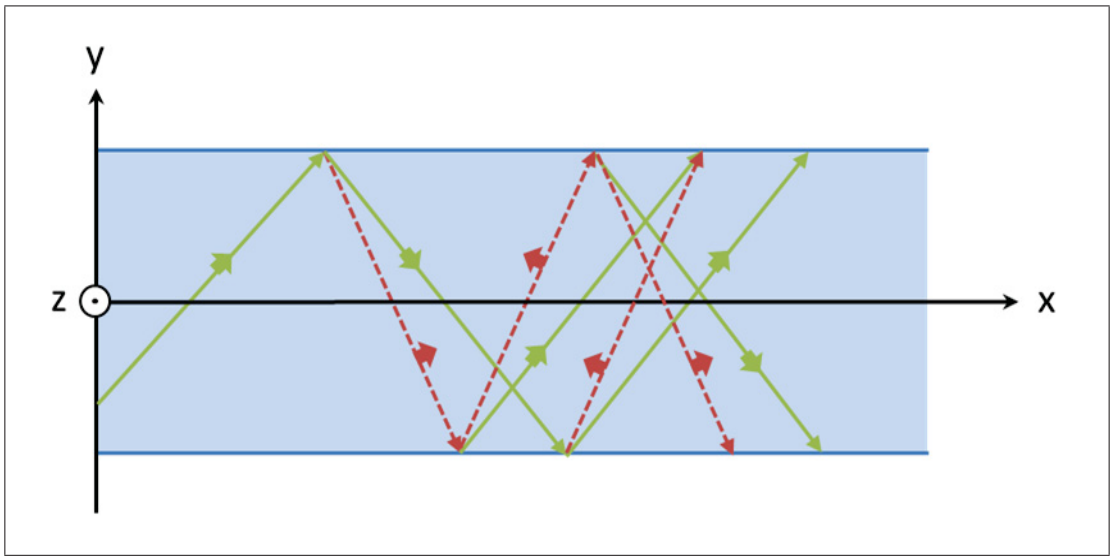

Figure 1.5 Bulk P-waves (green) and bulk SV wave (red) multiple reflections on the surfaces of a plate, leading to the propagation of Lamb waves

making the development of Lamb waves equations more complex is the mode conversion of both partial waves occurring at each reflection on the surface of the plate due to their non-zero normal to the plate surface displacement component (Krautkrämer and Krautkrämer (1990)). Figure 1.5 illustrates the propagation and the first reflections of the involved partial waves, resulting in the propagation of Lamb waves. This means that, to satisfy the traction-free surface conditions of the plates, the wave vector of both partial waves must share the same component in the propagation direction (Dieulesaint and Royer (1999)). Rewriting equation 1.12 for the two partial waves with this condition leads to

$$k_{y,L}^2 = \left(\frac{\omega}{c_L}\right)^2 - \ k_x^2, \tag{1.17}$$

$$k_{y,S}^2 = \left(\frac{\omega}{c_S}\right)^2 - \ k_x^2, \tag{1.18}$$

where, in both cases, the second term representing the partial waves' total wave vector, k_x, is still the shared wave vector component that represents the propagating Lamb wave, and, $k_{y,L}$ and $k_{y,S}$ represent the normal to the plate wave vector component of each partial wave.

Many excellent textbooks discuss the full detailed proof of the Rayleigh-Lamb equations that govern the Lamb wave propagation. That is why only the relevant steps will be discussed here (Lamb (1917)). To obtain these equations, one has to first apply the conservation relations at the boundaries of the plate on the normal component of the incident and the reflected waves for each partial wave. The next step is to express the four reflection coefficients in terms of the normal to the plate wave vector components to obtain the Rayleigh-Lamb wave equations, which are

$$\frac{\tan\left(k_{y,S}\,\frac{b}{2}\right)}{\tan\left(k_{y,L}\,\frac{b}{2}\right)} = -\frac{4\,k_x^2\,k_{y,L}\,k_{y,S}}{(k_{y,S}^2 - k_x^2)^2} \tag{1.19}$$

and

$$\frac{\tan\left(k_{y,S}\,\frac{b}{2}\right)}{\tan\left(k_{y,L}\,\frac{b}{2}\right)} = -\frac{(k_{y,S}^2 - k_x^2)^2}{4\,k_x^2\,k_{y,L}\,k_{y,S}}. \tag{1.20}$$

The dispersion relations of the Lamb waves are then obtained by combining equation 1.17

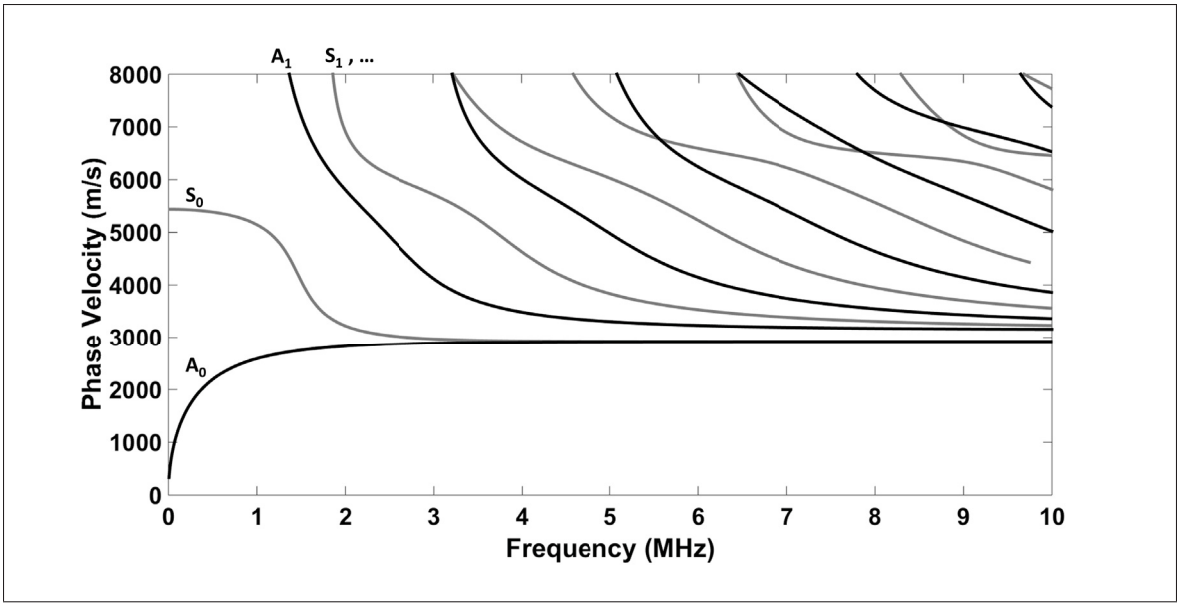

Figure 1.6 Phase velocity dispersion curves of Lamb waves in a 1.588 mm aluminum plate (E = 70.8 GPa, ν = 0.34, and ρ = 2700 kg/m^3), curves computed using DISPERSE software packages (Pavlakovic *et al.* (1997))

with equation 1.19 for the symmetric ($S_{n^{th}}$) modes and equation 1.18 with equation 1.20 for the antisymmetric ($A_{n^{th}}$) modes. The resulting relations are unfortunately transcendental and the eigenvalue problem that they represent has to be solved using numerical methods. The DISPERSE software package (Pavlakovic *et al.* (1997)), for example, does so. The same mathematical difficulties applies to the calculation of the dispersion relations of the group velocities, also requiring a numerical approach. Group velocity dispersion relations are obtained, again, by differentiating the dispersion relation function of the wavenumber and frequency with respect to the frequency. Figures 1.6 and 1.7 respectively illustrate the phase velocity dispersion curves and the group velocity dispersion curves in the same aluminum plate, as previously computed using the DISPERSE software package (Pavlakovic *et al.* (1997)).

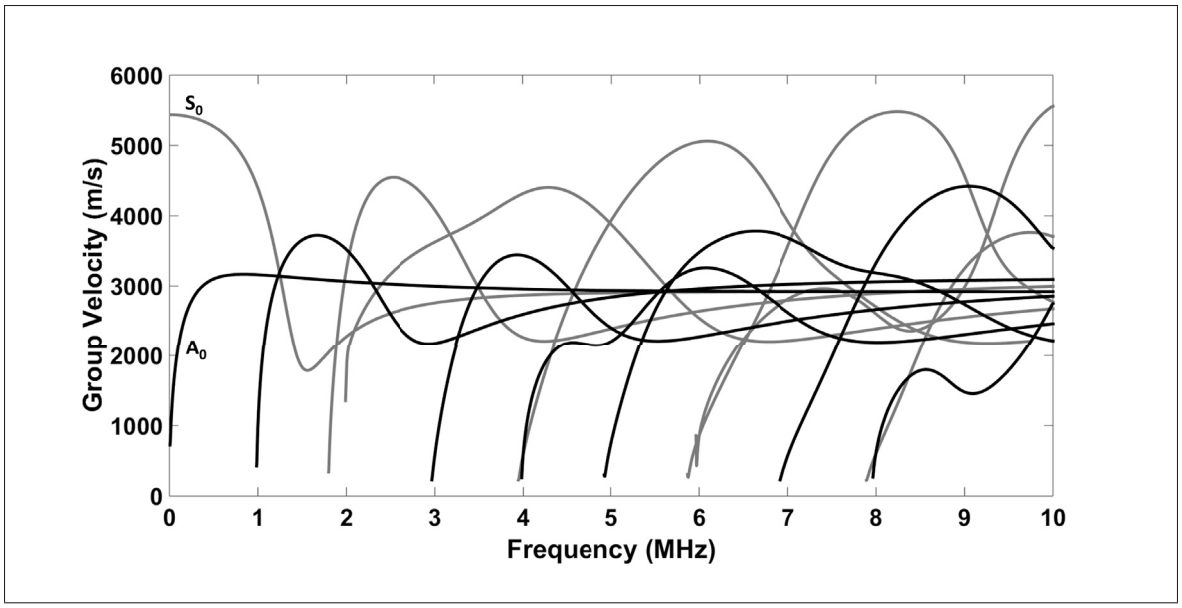

Figure 1.7 Group velocity dispersion curves of Lamb waves in a 1.588 mm aluminum plate (E = 70.8 GPa, ν = 0.34, and ρ = 2700 kg/m^3), curves computed using DISPERSE software packages (Pavlakovic *et al.* (1997))

1.2 Piezoelectricity Theoretical Background

Piezoelectricity was first discovered by the Curie brothers at the end of the nineteenth century quickly led to ultrasound applications. Piezoelectricity is an intrinsic electromechanical behavior of certain materials that accumulate electric charges when subjected to a mechanical load. This effect is called the direct piezoelectric effect, and is reversible, which is known as the converse piezoelectric effect, and results in a strain of the material when an electric field is applied to it. Piezoelectric ultrasonic transducers use the direct piezoelectric effect when they are being used as sensors and use the converse piezoelectric effect when they are being used as actuators. Many excellent textbooks discuss piezoelectricity (Nye (1957) and Jaffe *et al.* (1971)).

The piezoelectric effects can only take place in materials that have a crystal lattice for which the unit cell lacks, minimally, one symmetry plane crossing its geometric centre. This characteristic is called non-centrosymmetricity. Both piezoelectric effects are governed by the following

two constitutive equations:

$$D_i = \varepsilon_{ij}^T E_j + d_{ijk} T_{jk}, \tag{1.21}$$

and

$$S_{ij} = d_{ijk}^T E_k + s_{ijkl}^E T_{kl}, \tag{1.22}$$

where d is the piezoelectric coefficient tensor, ε is the dielectric constant, s is the compliance tensor, T is the state of stress, S the state of strain, D the electric displacement, E the electric field, and the superscripts T and E denote physical values measured under conditions of constant stress and a constant electric field, respectively.

Piezoelectricity is describe using a third-rank tensor, but its constants, here d_{ijk}^T, are often represented in a 3 x 6 matrix, easing the presentation. The transformed piezoelectric constant is therefore written d_{ij}^T, where subscript i goes from 1 to 3 and denotes the axis of the applied electric field, and subscript j goes from 1 to 6 and denotes the resulting strain; indexes 4, 5, and 6 stand for the shear strains. A piezoelectric material can be monocrystalline or polycrystalline. A monocrystalline material means that a sample is only constituted of a single and uniform crystal lattice, while polycrystalline material is constituted of an ensemble of crystals each called a grain.

Although the mathematics are simpler when considering monocrystalline materials, the same basic considerations apply to polycrystalline materials. Polycrystalline materials are discussed and used in this thesis with this understanding. Figure 1.8 illustrates a polycrystalline piezoelectric rectangular plate with the conventional piezoelectric axis and the six related possible strains with the third axis as the conventional polarization axis. A polycrystalline material is not considered macroscopically piezoelectric if it has not been poled by subjecting it to an intense electric field combined with an elevated temperature. This process is called poling and is required in order to align all the microscopic piezoelectric domains that are naturally randomly organized, resulting in a macroscopic net polarization. Another important characteristic of polycrystalline piezoelectric materials is that, once they are macroscopically poled, they are in a thermodynamically unstable state. This unstable state can be held for a certain

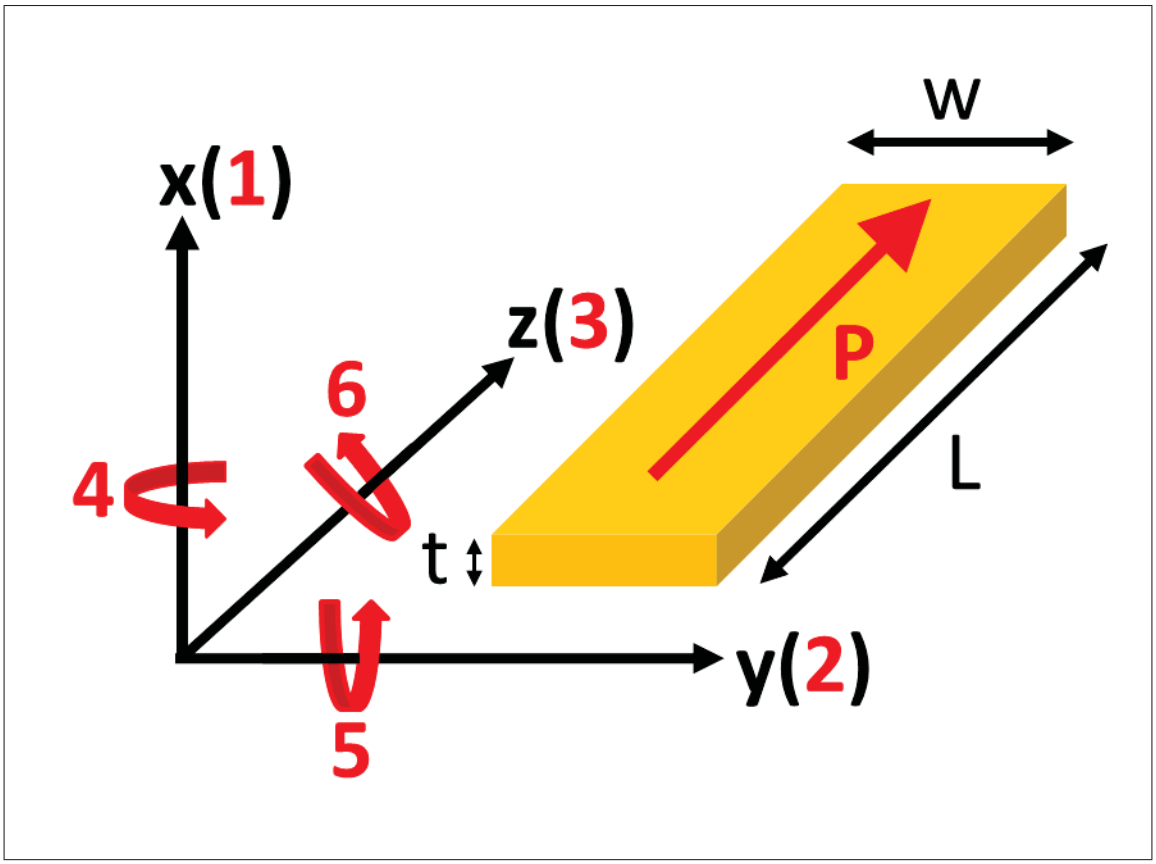

Figure 1.8 Conventional piezoelectric axes with the six possible related strains: typically, the polarization axis taken as along the 3^{rd} axis

amount of time that depends on many variables like time, temperature, and pressure but, in all cases, will tend to a non-macroscopically piezoelectric state after a finite time. Moreover, piezoelectric materials have a Curie temperature, for which the crystal structure will change to a centrosymmetric symmetry, yielding a material with no piezoelectric behavior.

1.3 Literature Review of SH_0 Transduction for SHM Applications

Structural health monitoring (SHM) consists of the continuous assessment of structural integrity using embedded systems. Ultrasound has been extensively used, first in the non-destructive evaluation (NDE) field, and then in SHM over the past two decades. Bulk ultrasounds were first used in NDE to characterize material properties, evaluate material thickness,

or coating thickness, and to detect defects like volume flaws or composite delamination. Later, plate-guided waves were found to be of great interest for their ability to propagate over long distances in bounded media, including plates, allowing the faster scanning of large surfaces than with conventional ultrasound techniques. The dispersive aspect of plate-guided waves represents, however, a big technical challenge. Moreover, existence of high-order modes tends to limit the choice of frequency to frequencies below the first cut-off frequency to avoid the propagation of high-order modes. Researchers have developed many techniques to limit the undesirable characteristics of guided waves, like limiting the frequency of inspections (Cawley and Alleyne (1996)), dealing with dispersion using the compensation method, or trying to control the generated modes (Ostiguy *et al.* (2012)).

Despite all these technical challenges, guided-wave NDT techniques are now widely spread and used in industries, such as energy or transport (Cawley *et al.* (2003) and Wilcox *et al.* (2003)). Lamb waves were intensively studied and used especially because of their relatively straightforward generation mechanism. In fact, all Lamb modes have a non-zero normal to the plate displacement component at any given frequency, leading to the generation of all possible Lamb modes with a simple normal excitation. On the other hand, researchers had to deal with this ease of generation when they attempted to develop a mode selective transducer (Clarke *et al.* (2009)). In this work, the author's objective was to generate the fundamental antisymmetric Lamb mode (A_0) at a high level of purity at low frequencies. In order to do so, they started with a conventional thickness poled lead zirconate titanate (PZT) sample, which is a commonly used hard piezoelectric ceramic, thus exploiting the thickness extension vibration mode. To achieve their goal, they used silicon carbide foam as the wear plate of their transducer, in order to suppress the undesired parallel-to-the-plate displacement component that comes from the Poisson effect at which, at low frequencies, the fundamental Lamb symmetric (S_0) mode is very sensitive. They successfully generated the desired A_0 mode at 40 dB over the undesired S_0 mode with the use of this adapted wear plate and simple geometric considerations.

1.3.1 Piezo-ceramic Transduction

Piezoelectric ceramic transducers use the previously described piezoelectric effect in order to generate or to detect ultrasound. In the case of the generation of the fundamental SH mode (SH_0), a surface shear stress source must be used. In a study by Rajagopal and Lowe (2007), a conventional commercial ultrasonic round shear transducer originally designed for bulk wave applications was used. They demonstrated that using such a transducer to produce the SH_0 mode works fine, but it also unfortunately generates the S_0 mode at a level of amplitude comparable to the SH_0 mode, as well as the A_0 mode, at a lower amplitude. Moreover, because of their low ratio of active element size to the wavelengths covered by their bandwidth, such transducers act as point sources. This leads to the generation of perfect dipole patterns, characterized by wide wave field apertures, and to further interferences of the propagating modes. This solution is suited to localized uses of the SH_0 mode in well-controlled conditions in order to avoid or control the propagation of the Lamb modes and thus the possible reflections of the Lamb modes that, if not, might interfere with the SH modes.

Kamal and Giurgiutiu (2014) used a commercial shear plate supplied by American Piezo Ceramics (APC) International, Ltd. (americanpiezo.com) to generate SH waves, including high-order modes. The shear plate was made out of PZT and was square in shape. The electric field was applied across the thickness of the plate (third piezoelectric axis) and the shear motion was obtained via the d_{35} piezoelectric coefficient. The geometry was not optimized to produce the desired waves, and the excitation frequency was chosen according to the imposed supplied geometry. The results showed that, again, this solution is suited for the generation of low-frequency SH waves, but it appears to also generate Lamb modes at very high levels of amplitude. Using such a material in such conditions cannot represent an ideal solution to generate a SH wave at a high level of purity because three vibrational modes other than the desired one are also involved via d_{31}, d_{32}, and d_{33}, which are far from being negligible for hard ceramics like PZT. This aspect was not taken into account in this paper. The same kind of solution was used by Zhou *et al.* (2015), but they used lead magnesium niobate titanate (PMNT) as the piezoelectric material. They performed a (011) plane cut of the material to obtain their

shear plate. This manipulation allowed them to obtain a very high d_{36} piezoelectric coefficient (-1648 x 10^{-12} m^2 N^{-1}), which is at least 1.85 times higher than the resulting d_{31}, d_{32}, and d_{33}, compared to 1.48 higher in the previous study. However, such a design is still not suited to maximize the generation of the SH_0 mode.

Another way to use piezoelectric ceramics to produce SH waves is the use of an array of sensors, as discussed by Wilcox *et al.* (2000). This solution is made of multiple piezoceramic square shear actuators assembled into a chessboard pattern. This way, the central frequency is dictated by the geometry of the array, and a plane wave can be easily generated due to the total length of the array. Generation of both fundamental Lamb modes at the tips of the array was not discussed in this work for this configuration. Again, this solution, due to the number of elements, the alignment complexity, and its bulkiness, is not suited for SHM applications.

1.3.2 Electromagnetic Acoustic Transducer

Another completely different method that can be used to generate SH waves is the electromagnetic acoustic transducer (EMAT), which is based on the Lorentz forces that are generated within a material that is subjected to eddy currents and also subjected to a permanent magnetic field to produce ultrasounds. The advantage of EMAT is that it is a purely non-contact solution. However, it requires much higher input power to induce sufficient energy in the media, and the media must be an electrical conductor; alternatively, a conductive patch (also called a magnetostrictive patch) must be bonded to the plate, eliminating the non-contact advantage.

The orientation of the permanent magnetic field with respect to the plate dictates the orientation of the generated Lorentz forces within the plate. If the magnetic field is parallel to the plate, then normal forces are generated, and if it is normal to the plate, shear forces are generated. Due to the importance of the alignment of both the permanent magnetic field and the coil responsible for the induced eddy currents in the plate with respect to the plate, it is very difficult to predict precisely the resulting induced force field in the plate. Another limitation of the use of EMATs is the penetration depth of the eddy currents: in fact, the penetration depth of the eddy

currents depends on the material properties and the frequency of excitation, as do the Lorentz forces. Indeed, this aspect must be considered because of the non-constant through-thickness displacement profile of all guided-wave modes, except SH_0, which is constant. Therefore, the frequency must be chosen for a given conductive material in order to control the penetration depth and thus obtain better control of the generated modes. Two other difficulties of using EMAT to generate ultrasonic waves are that it is crucial that the liftoff (the distance between the media and the device) remains the same for a matter of repeatability and that, since the design frequency is related to the spacing and the number of the coil that generates the eddy currents in the plate, the bandwidth of these types of probes appears to be very limited as the coil requires many turns to compensate for the low efficiency of the energy transduction.

For almost 40 years now, EMATs have been used in studies to create SH waves, such as in the work of Thompson *et al.* (1972). In fact, it appears that these types of waves produced by EMATs have been of increasing interest, as in the work of Böttger *et al.* (1987), Wilcox *et al.* (2005), Hiroa and Ogi (1999) and Qingzeng *et al.* (2014), due to the simple configuration required and, as in this work, due to the numerous advantages of having a single wave mode with a pure displacement polarization propagating in the medium.

1.3.3 Piezoelectric Polymer Transducer

Another option discussed in the literature in order to generate or receive plate-guided waves is the use of piezoelectric polymers as the transduction material, such as polyvinylidene difluoride (PVDF) (Wilcox *et al.* (1998)). These types of materials have the advantage of being flexible. However, piezoelectric polymers exhibit a very low electromechanical coupling coefficient, which is around 10% compared to 50% for hard ceramics like PZT. This characteristic combined with their relatively low piezoelectric coefficients, ranging from about 6 x 10^{-12} to 30 x 10^{-12} m^2 N^{-1} compared to almost a 1,000 for PZT, contributes to the limited interest in this type of material. Moreover, the fact that polymers generally have a very low melting temperature (about °C for PVDF) seems to have discouraged such materials for conventional NDT or SHM applications.

Due to the previously stated limitations of polymeric materials like PVDF, the very few times piezoelectric polymers have been investigated to generate guided waves, they were used as interdigitated PVDF transducers (Monkhouse *et al.* (1997)). This type of configuration is characterized by an array of multiple fingers of PVDF fibres. Many fingers are necessary in order to transmit a sufficient amount of energy for testing to be practicable. The spacing and polarization of each finger, all in the same direction or in an alternating opposite direction, dictates the generated mode and central frequency that can be generated for a given configuration. Therefore, the same problem that occurs with EMATs, a limited bandwidth, is observed.

CHAPTER 2

ARTICLE: DEVELOPMENT OF A LOW-FREQUENCY PIEZO-CERAMIC TRANSDUCER FOR THE GENERATION OF PLANE SHEAR HORIZONTAL GUIDED WAVES

Guillaume Boivin[1], Martin Viens[1], Pierre Belanger[1]

[1] Département de Génie Mécanique, École de Technologie Supérieure,
1100 Notre-Dame Ouest, Montréal, Québec, Canada H3C 1K3

This article was submitted to the journal *Ultrasonics* in July 2016

2.1 Abstract

The shear horizontal (SH) guided wave fundamental mode (SH_0) has the particularity of being the only non-dispersive guided wave mode in plates. This characteristic makes this ultrasonic guided wave mode very attractive for structural health monitoring (SHM) applications, facilitating signal processing for long range inspections. However, the generation of a single guided wave mode when using piezoelectric transduction is very challenging. The aim of this work is to develop a piezo-ceramic transducer optimized for the generation of plane zeroth order SH waves and to minimize both fundamental Lamb modes using geometric considerations. The chosen material was the PZT-5H because of its dominant d_{15} piezoelectric constant, which makes it a perfect candidate for SH wave generation using thickness-shear motion. The transducer dimensions were first optimized using an analytical model. A 3D multiphysics finite-element model was then used to validate the analytical model results. Experimental validation was finally conducted with a laser Doppler vibrometer (LDV) system on one of the four previously determined optimized designs. Excellent agreement between the analytical model, finite-element model, and experimental validation were observed, confirming the possibility of generating the SH_0 mode at a high level of purity using piezo-ceramic transduction as well as optimized geometry.

2.2 Introduction

Conventional ultrasounds have now been used for decades in non-destructive testing (NDT) whether for material characterization or non-destructive evaluation (NDE). More recently, ultrasonic guided waves have attracted NDT researchers for their ability to propagate over long distances in thin structures. This feature has allowed the development of many novel techniques that are now routinely used in the inspection of pipelines and pressure vessels (Staszewski *et al.* (2004); Raghavan and Cesnik (2007); Croxford *et al.* (2007)).

Structural health monitoring consists of the permanent implementation of NDE solutions rather than proceeding systematically to periodic testing. One way to achieve this purpose is to permanently attach specifically designed transducers to assess the structure of interest. The requirements for these transducers are typically to have a minimal footprint, low weight, and the ability to survive harsh operating conditions (Raghavan and Cesnik (2007); Ostiguy *et al.* (2012)).

Low-frequency excitations have primarily been used in NDT and SHM applications involving guided waves because of the number of modes propagating at high frequency (Cawley *et al.* (2003)), thus allowing longer range inspections by limiting the undesired effect of multiple dispersive guided wave modes propagating. In fact, the required signal processing as well as the inspection complexity is drastically reduced. A different approach to increase the inspection range and minimize post-processing time is to use the fundamental SH mode (SH_0). Indeed, SH_0 exhibits two interesting characteristics: 1) it has no attenuation due to fluid loading of the structure and 2) it is the only non-dispersive guided wave mode in plates (Alleyne *et al.* (2004)).

This project focuses on the development of a low-frequency piezo-ceramic transducer for the generation of the fundamental SH mode (SH_0) to be used in SHM applications. Different solutions have been developed to do so, such as polyvinylidene difluoride (PVDF) interdigital transducers (Belanger (2013); Monkhouse *et al.* (1997)) or electromagnetic acoustic transduc-

ers (Ribichini *et al.* (2011); Hiroa and Ogi (1999)). These solutions are, however, not suited for low-frequency SHM applications due to the difficulty of embedding the devices in the structure.

This paper first presents the theoretical background of piezoelectricity, and vibrational mechanisms in order to select the proper material to generate the SH_0 mode. The two geometric parameters used to optimize the generation of the desired mode are then discussed. The third part presents the wave-propagation analytical model used to validate the chosen geometry which is then validated using the Abaqus finite-element software package. Finally, the fourth section presents the experimental validation of the designed transducer.

2.3 Theoretical Background

Ultrasonic guided waves are one type of mechanical stress wave that can propagate in solid plate-like media. These ultrasonic waves can be grouped into two classes: Lamb waves (symmetrical and antisymmetrical modes) and SH waves. For each class, fundamental and high-order modes can exist. Fundamental modes exist at any frequency-thickness product while high order modes appear at specific frequency-thickness product known as the cut-off frequency-thickness product (Rose (1999)). Unlike bulk ultrasonic waves in isotropic solids, the velocity of ultrasonic guided waves changes with the frequency; this phenomenon is called dispersion. Figure 2.1 presents the phase velocity dispersion curves in a 1.59 mm aluminum plate (E = 70.8 GPa, ν = 0.34, and ρ = 2700 kg/m^3) computed using the DISPERSE software package (Pavlakovic *et al.* (1997)).

This plate thickness and material are used in the remainder of this paper. Figure 2.1 illustrates that the only non-dispersive guided wave mode in a plate is the fundamental SH mode, SH_0.

Inspection frequencies are typically chosen below the cut-off frequency-thickness product of the first high-order modes, thus significantly reducing the required signal processing complexity. Limiting the frequency has the benefit of limiting the effect of attenuation, hence enabling long range inspections (Dieulesaint and Royer (1999)). In addition, SH waves present very low energy leakage in the surrounding medium compared to Lamb waves due to the absence

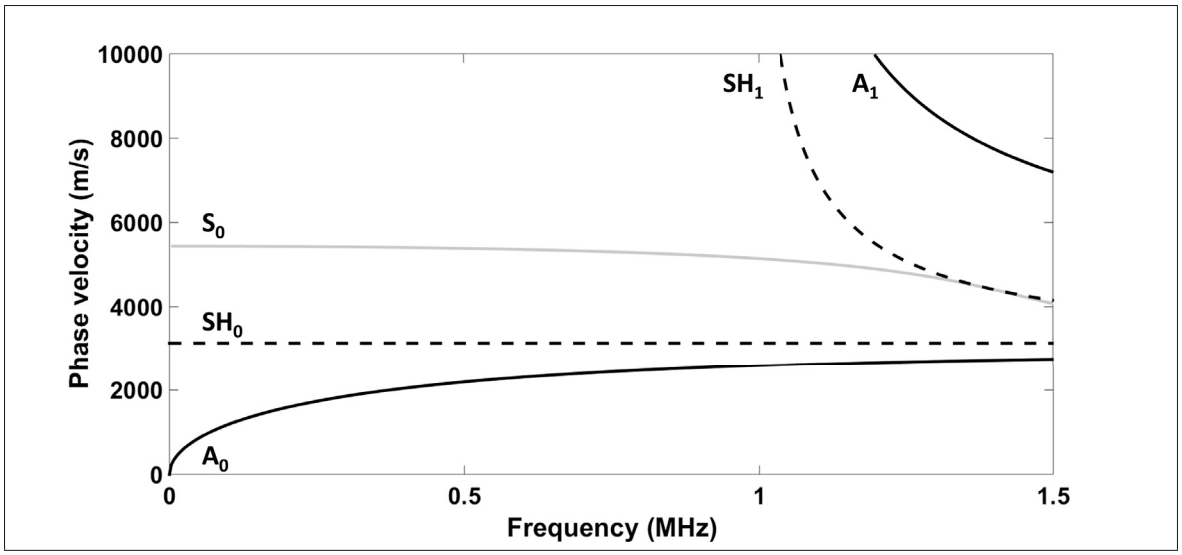

Figure 2.1 Phase velocity dispersion curves in a 1.59 mm aluminum plate (E = 70.8 GPa, ν = 0.34, and ρ = 2700 kg/m^3). The solid black lines correspond to the A_0 and A_1 modes, the solid light-grey lines correspond to the S_0 mode and the dashed black lines correspond to the SH_0 and SH_1 modes

of particle motion normal to the plate. Unfortunately, low-frequency limits the resolution of the inspections that can be performed, as the resolution is directly related to the propagating wavelength.

In order to generate ultrasounds in a medium, strain must be induced. The generated ultrasonic modes thus depend on the type of strain that is induced in the medium as well as the excitability of each mode (Belanger (2009)).The SH_0 mode is the only fundamental mode with particle motion perpendicular to the propagation direction and parallel to the plate and is also the only fundamental mode with a single component of particle motion. Figure 2.2 illustrates these particle motions for each fundamental mode. Both fundamental Lamb modes exhibit a quasi-pure polarization at low frequencies: z direction for A_0 mode and x direction for S_0 mode in Figure 2.2. A y-direction shear strain is required to generate a SH_0 wave. Figure 2.3 shows the directivity pattern of the acoustic field resulting from an in-plane shear point source for each fundamental mode. Unfortunately, as it can be seen in Figure 2.3, the required excitation results in the generation of both fundamental Lamb modes in the direction of excitation following a

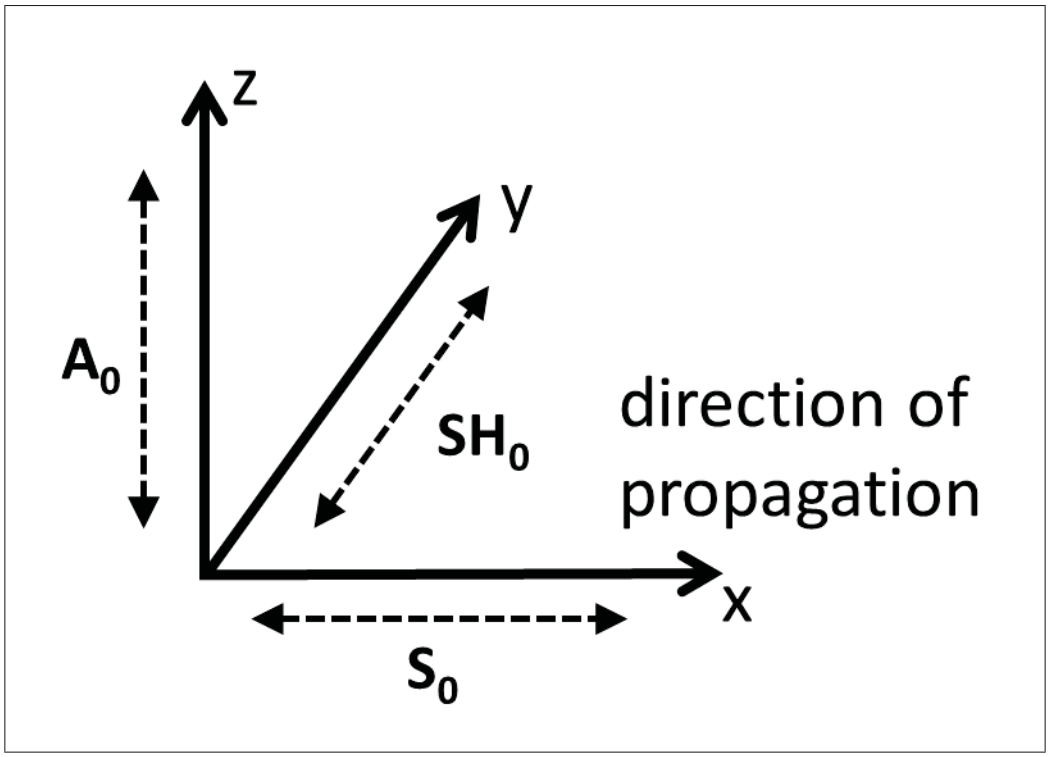

Figure 2.2 Schematic of the dominant particle motion of each fundamental mode at low frequency according to the direction of propagation (here in the positive x direction); SH_0 has a pure motion polarization regardless of the frequency, while both fundamental Lamb modes have quasi-pure motion polarization at low frequencies

dipole pattern for which the two directivity lobes are in opposition of phase (Belanger (2013)). On the other hand, SH modes are generated perpendicular to the excitation direction, also following a dipole pattern for which the two directivity lobes are in phase.

Piezoelectric acoustic transducers use the converse piezoelectric effect to generate strain when submitted to an electric field. Therefore, the first step in the development of a precise transducer is to choose the proper material that will generate the desired strain. Three fundamental vibrational modes can be used to obtain a surface shear strain in a plate-like piezoelectric sample: thickness-extensional mode via Poisson effects, length or width-extensional mode, and thickness-shear mode (Buchanan (1956)). Figure 2.4 shows the three modes of deformation. The preferred mode clearly appears to be the thickness-shear with a single shear motion with-

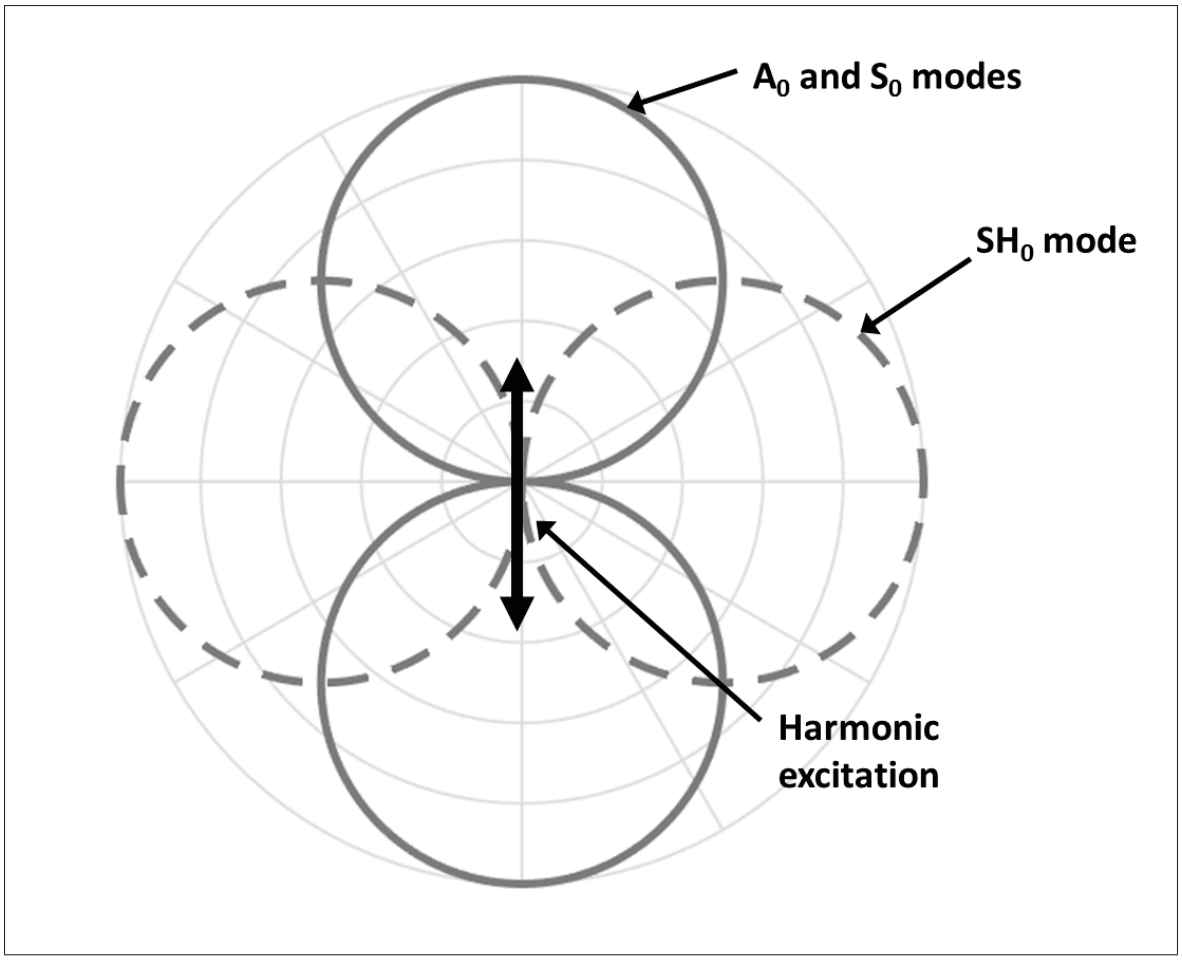

Figure 2.3 Directivity pattern of a harmonic surface shear stress point source. The dashed light-grey lines represent the SH_0 mode that propagates normal to the excitation direction, and the solid light-grey lines represent the A_0 and S_0 modes, which propagate parallel to the excitation direction

out any unwanted Poisson effects. Assuming a polycrystalline ferroelectric material and the geometry of Figure 2.5, the thickness-shear mode can be obtained via six different combinations of poling and piezoelectric constants d_{ij} for every non-equal i and j. Using this notation, subscript i denotes the corresponding sample thickness axis (where the electric field is applied) and subscript j denotes the axis corresponding to the length of the sample, knowing that the conventional piezoelectric polarization axis is the third one. Following this assumption, the ideal material would only exhibit one of the six d_{ij} coefficients with all others (d_{ikl}) equal to zero. Only four crystal classes exhibit this precise configuration: orthorhombic mm2 class,

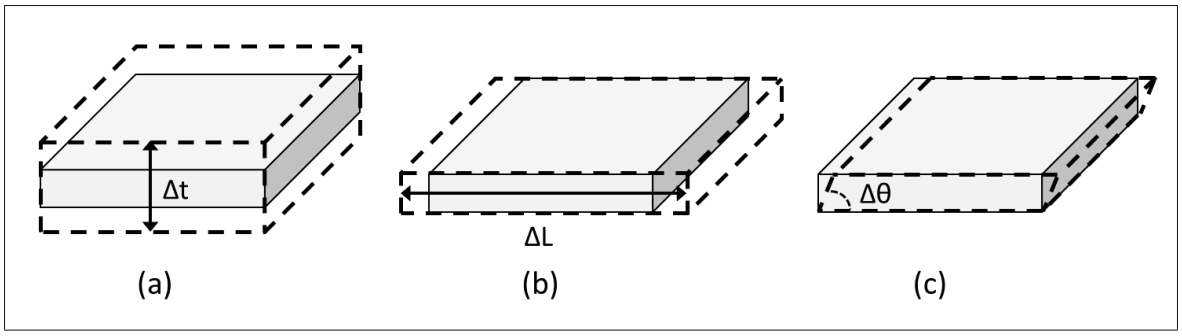

Figure 2.4 Displacement modes of a piezoelectric plate allowing SH wave generation: (a) thickness-extensional displacement mode, (b) length-extensional displacement mode, and (c) thickness-shear displacement mode

tetragonal 4mm class, and hexagonal 6mm and $\bar{6}$m2 classes. Very few materials exhibit such a stable structure at room temperature (Nye (1957)). Lead zirconate titanate (PZT) belongs to the tetragonal 4mm class under its Curie temperature if the $PbTiO_3$ mol% is greater than 50%. The piezoelectric matrix of the PZT-5H is:

$$d = \begin{vmatrix} 0 & 0 & 0 & 0 & 730 & 0 \\ 0 & 0 & 0 & 730 & 0 & 0 \\ -265 & -265 & 530 & 0 & 0 & 0 \end{vmatrix} 10^{-12} \frac{C}{N}.$$

,

The detailed PZT-5H material properties can be found on the supplier website (http://bostonpiezooptics.com). This specific PZT was the chosen material for this work because of its only independent coefficient, which is d_{113} (d_{15}), greater than any other PZT composition.

In order to maximize the generation of a plane SH wave and to minimize the generation of Lamb waves, the optimization of specific geometric parameters of the piezoelectric sample is important. Two geometric parameters are of great interest for the generation of guided waves. The first one is the ratio of the length of the sample in the direction of propagation of a mode, the width w for the SH_0 mode and the length L for the Lamb modes according to Figure 2.5, over the wavelength of this mode. Indeed, this parameter governs the maximum amplitude that

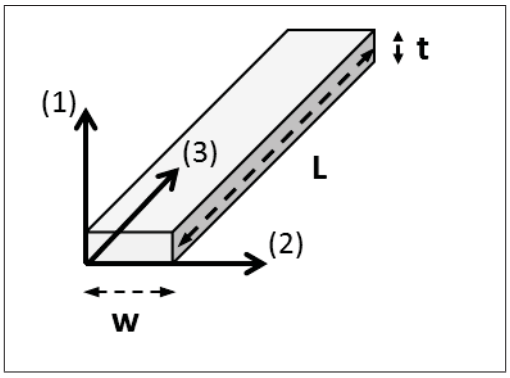

Figure 2.5 Coordinate system related to the purchased piezoelectric samples from Boston Piezo-Optics. The sample is poled along the third axis, and the electrodes are on the faces normal to the first axis. Geometric parameters *L*, *w* and *t* will be used as reference in this paper

can be generated as a function of frequency for a particular mode in the manner of a vibrational resonator. Thus, the first resonant frequency will occur for a mode wavelength equal to twice the related size of the transducer, and harmonics will occur for every odd multiple of this mode wavelength (Cheeke (2012)). In the same way, if the ratio of the length over the wavelength corresponds to an integer, the mode amplitude would then be zero.

The second important geometric parameter is the ratio of the propagating wavelength over the distance perpendicular to the propagating direction, L for the SH_0 mode and w for both fundamentals Lamb modes. This ratio governs the aperture of the generated beam. According to the far field propagation theory, if the ratio λ/L is greater or equal to one, the source will act as a dipole (Figure 2.3) and only the main lobe will exist. On the other hand, when this ratio becomes smaller than one, the aperture tends to reduce, but the side lobes of lower amplitudes start to appear (Jensen (2002)). Thus, to obtain a plane SH_0 wave, the length of the transducer must be minimally greater than the propagating SH_0 wavelength to focus the main lobe of the SH_0 mode. In the same way, the perfect situation would be that both Lamb modes wavelength would be equal or smaller to the width of the transducer so that their main lobes would be focused and, thus, only their side lobes, of smaller amplitudes, would interfered with the SH_0 wave.

2.4 Simulations

As poling is a critical and difficult to achieve step, PZT-5H rectangular plate (L = 25.4 mm, w = 50 mm, t = 1 mm), poled by the manufacturer in the L direction, was bought directly from Boston Piezo Inc. The L dimension was the maximum poling length available because of the technical difficulty that it implies, due to the extremely high dc voltage required, resulting in too great uncertainty in the average poling for large samples. The imposed maximum length restricts the maximum length of the transducer; thus, the minimum frequency design at 213 kHz, as S_0 mode wavelength is greater below this frequency, it would then be impossible to satisfy the first criterion. Classical bulk ultrasonic transducers are designed to work at higher frequencies where the wavelength over the transduction surface length ratio is necessarily way below unity, fully satisfying the plane wave approximation. It is, however, not the case in this precise application due to the low-frequency requirement to avoid high-order modes. For this reason, in order to maximize the SH_0 plane wave generation, the length L of the transducer was fixed to 25.4 mm.

The in-plane excitability of the S_0 mode being, by far, greater than that of A_0, the focus was put on the minimization of the S_0 mode using the first criterion (Belanger (2009)). With a fixed length of 25.4 mm, four frequencies between 213 kHz and the first cut-off frequency fully satisfy this criterion for the S_0 mode: 213 kHz, 425 kHz, 631 kHz, and 829 kHz, which correspond respectively to one to four S_0 wavelengths in the length of the transducer. The corresponding length over the A_0 wavelength ratios are then 3.33, 5.17, 6.86, and 8.44, and the corresponding SH_0 half wavelengths, dictating the transducer width are 7.4 mm, 3.7 mm, 2.5 mm, and 1.9 mm.

2.4.1 Analytical Simulations

Wave-propagation finite-element simulations can be extremely computer intensive, especially when studying both Lamb and SH modes requiring 3D models (Belanger (2013)). For this particular reason, the two geometric criteria were first optimized using a wave-propagation

analytical model and then a subset of the analytical simulations was validated against a finite-element model. This model is based on the Huygens' superposition principle combined with the dipole pattern assumption of a shear point source, previously stated. Using this model, the resulting total displacement field due to a discretized excitation is obtained with:

$$u(r,\theta,t) = \frac{sin(\theta)}{2\pi} \sum_m \int_{-\infty}^{+\infty} A(\omega) E_m(\omega) H_0^{(1)}(k(\omega)r) e^{i\omega t} d\omega, \tag{2.1}$$

where $A(\omega)$ is the complex amplitude of excitation, $E_m(\omega)$ is the in-plane excitability of the m_{th} mode, $H_0^{(1)}$ is the Hankel function of the first kind, and the term $\sin(\theta)$ represents the dipole directivity of the SH mode (this term changes to $\cos(\theta)$ for the Lamb modes). The excitation area was discretized using a minimum of four point sources per propagating wavelength (Wilcox *et al.* (1998)).

Figure 2.6 illustrates the directivity patterns of the four previously stated geometries using the analytical model. The directivity patterns are presented as a function of the corresponding propagating wavenumber non-normalized amplitude. The modes' excitabilities, $E_m(\omega)$, to a shear excitation on the surface of a plate were determined using both the DISPERSE software package and finite-element simulations for every desired frequency. A five cycle Hann-windowed toneburst centred at each frequency was used as the excitation signal. As expected, the SH_0 wave field becomes narrower with increasing frequency for a fixed length, but its reduction in amplitude is due to the reduction of the total transduction area. The A_0 beam, as expected, in all the cases, is at a minimum of 26 dB under SH_0 due to the poor excitability of this mode at such low frequencies. The S_0 directivity changes considerably with an increase of the frequency. Indeed, at the lowest frequency (213 kHz), only the main lobe can be observed, while side lobes appear gradually from 425 kHz to 829 kHz with the focusing of the main lobe. As observed, the desired effect of the first geometric assumption is only effective at angles close to the propagating direction of the modes. Increasing the frequency leads to a reduction of the aperture of the main lobe that will be minimized but, unfortunately, also leads to lower amplitude side lobes that cannot be minimized.

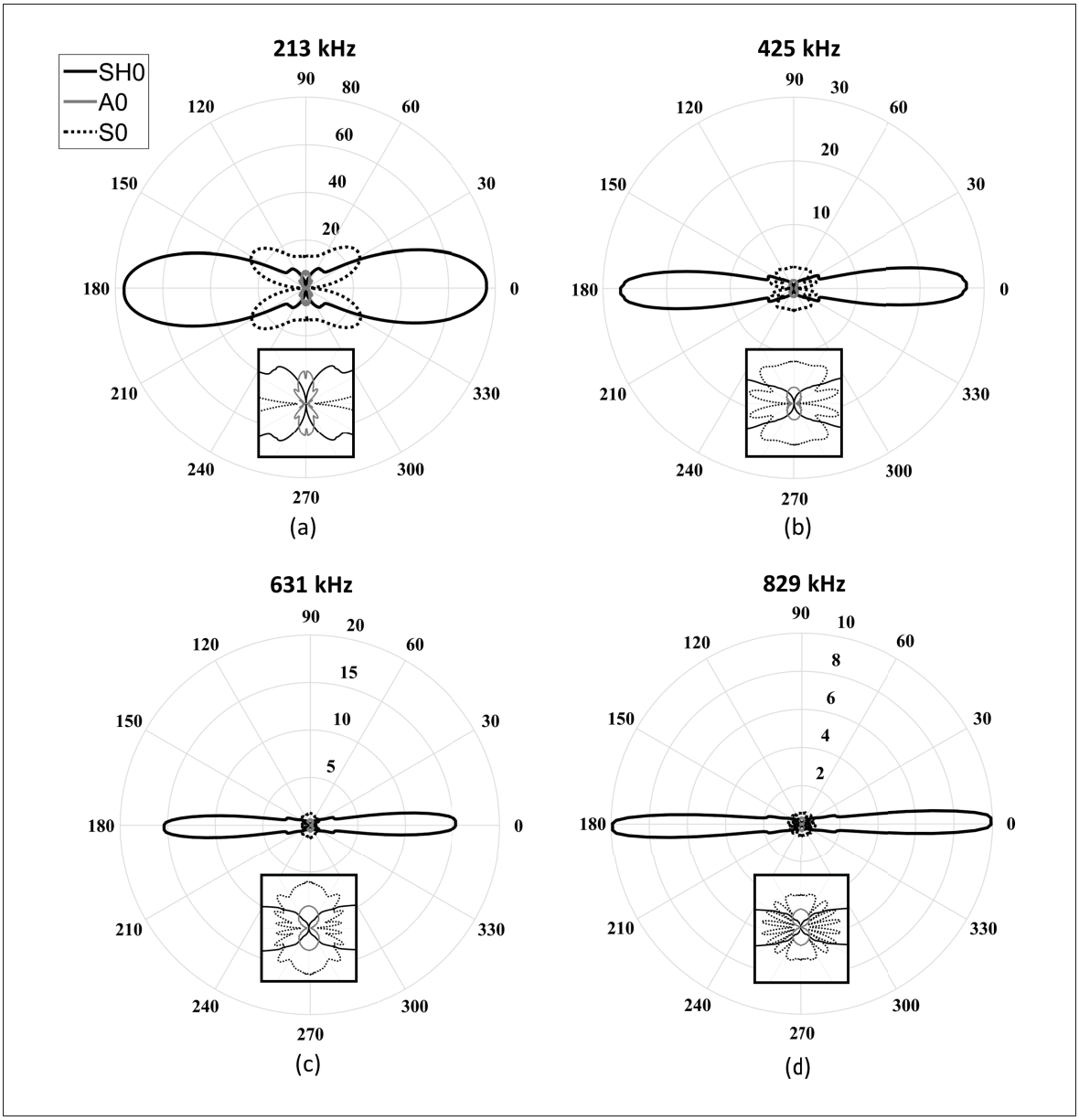

Figure 2.6 Directivity patterns of the fundamental modes obtained from the analytical model. The solid black lines represent the SH_0 mode, the dashed black lines represent the S_0 mode and the solid grey lines represent the A_0 mode. Directivity patterns for a five cycles Hann-windowed toneburst centred at (a) 213 kHz, (b) 425 kHz, (c) 631 kHz, and (d) 829 kHz

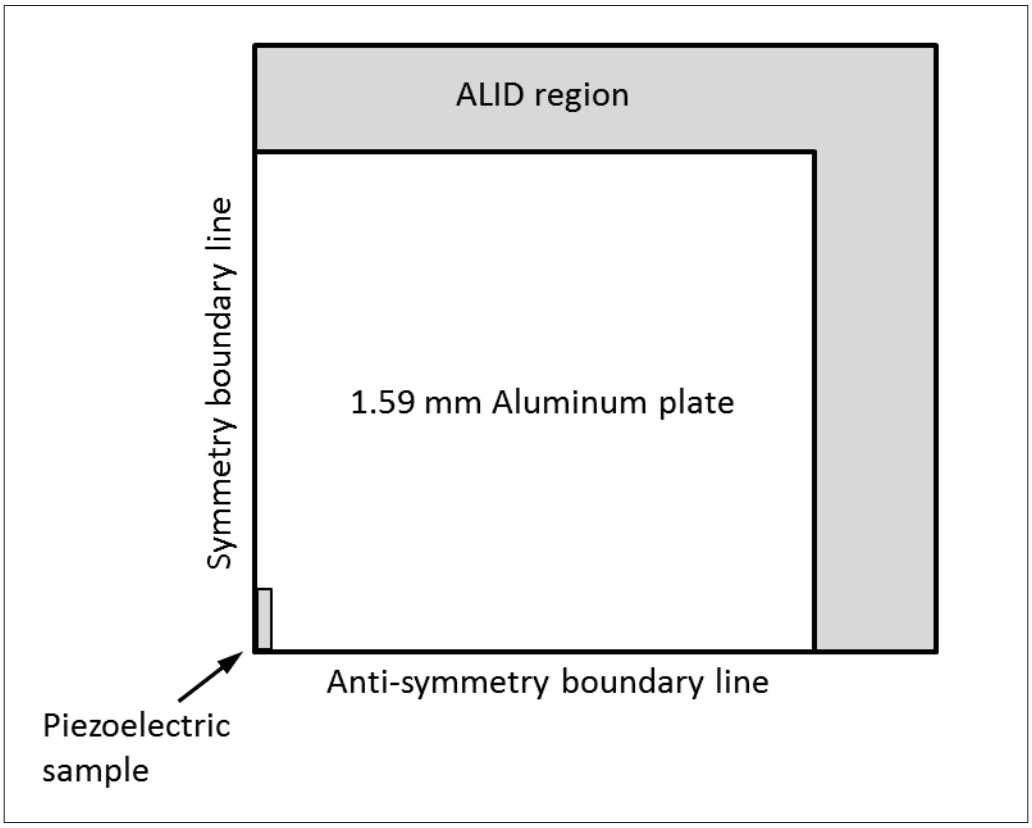

Figure 2.7 Reduced finite-element scheme of a quarter plate. Symmetry boundary line is used in the Lamb mode propagation direction, while thr anti-symmetry boundary line is used in the SH mode propagation direction. Absorbing layers with increasing damping (ALID) regions were used to avoid reflection from edges

2.4.2 Finite-Element Simulations

Wave-propagation simulations were then performed using the finite-element analysis commercial software Abaqus to validate the results of the analytical model. The 3D finite-element models were used, combining absorbing layers with increasing damping (ALID) region and symmetry and antisymmetric boundary lines in order to avoid undesired wave reflections and to reduce the model size and thus the computational time Drodz *et al.* (2006). The ALID region lengths were of at least five times the greatest propagating wavelength to fully absorb the propagating waves Drodz *et al.* (2006). A schematic of the model is presented in Figure 2.7. To avoid numerical errors, ten elements per the smallest propagation wavelength were

used Mohamed and Masson (2010). Spatial fast Fourier transform (FFT) was performed on the series of incident angles, and directivity patterns were then obtained by looking at the propagating wavenumbers according to the proper displacement component: in-plane radial for the S_0 mode, in-plane normal for the SH_0 mode and out-of-plane for the A_0 mode.

Figure 2.8 illustrates the directivity patterns obtained by finite-element simulations. The lowest frequency design reveals that the SH_0 wave field aperture was slightly underestimated with the analytical model, while S_0 and A_0 wave fields appear to be of the same shape but at twice the expected amplitudes. The design at 425 kHz wave fields appears to be similar to those predicted using the analytical model, except for the A_0 mode amplitude, which is slightly higher than expected but still very low compared to SH_0. This can be explained by the effect of the moving mass of the transducer that was neglected in the analytical model. This pendulum-like movement adds an undesired normal component of displacement that explains the higher amplitude of the A_0 mode for which the z direction excitability is high (Figure 2.2). The final two studied geometries present similar wave fields to the analytical model with higher amplitudes of the side lobe of the SH_0 wave field at 829 kHz. The same pendulum effect is also observed in both final frequencies, explaining the A_0 higher than expected amplitude but, again, is still very low compared to the SH_0 mode.

Dynamic response analysis of the different sizes was finally performed using Comsol Multiphysics 5.0 software. The first electromechanical resonance frequency, in this case, the thickness-shear fundamental, appears around 450 kHz and is independent of the width and slightly dependent on the mass addition that could come, for example, from a wear plate or backing mass that could be required for particular applications. For this reason, the design frequency was chosen to be 425 kHz, as the thickness-shear motion is dominant in this frequency range.

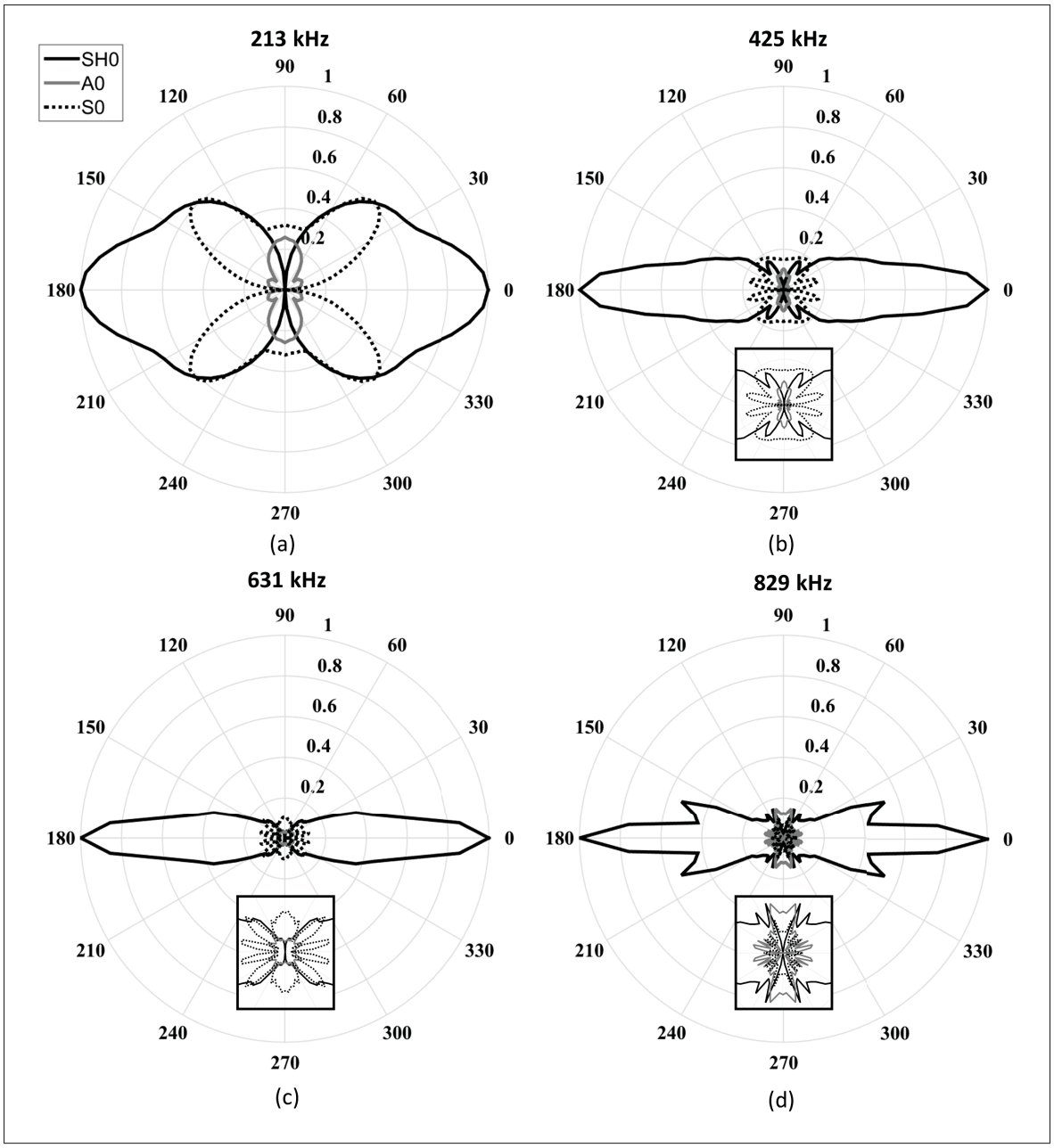

Figure 2.8 Directivity patterns of the fundamental modes obtained from finite-element simulations. The solid black line represents the SH_0 mode, the dashed black line represents the S_0 mode, and the solid light-grey line represents the A_0 mode. Directivity patterns for a five cycles Hann-windowed toneburst centred at (a) 213 kHz, (b) 425 kHz, (c) 631 kHz, and (d) 829 kHz

2.5 Experimental Validation

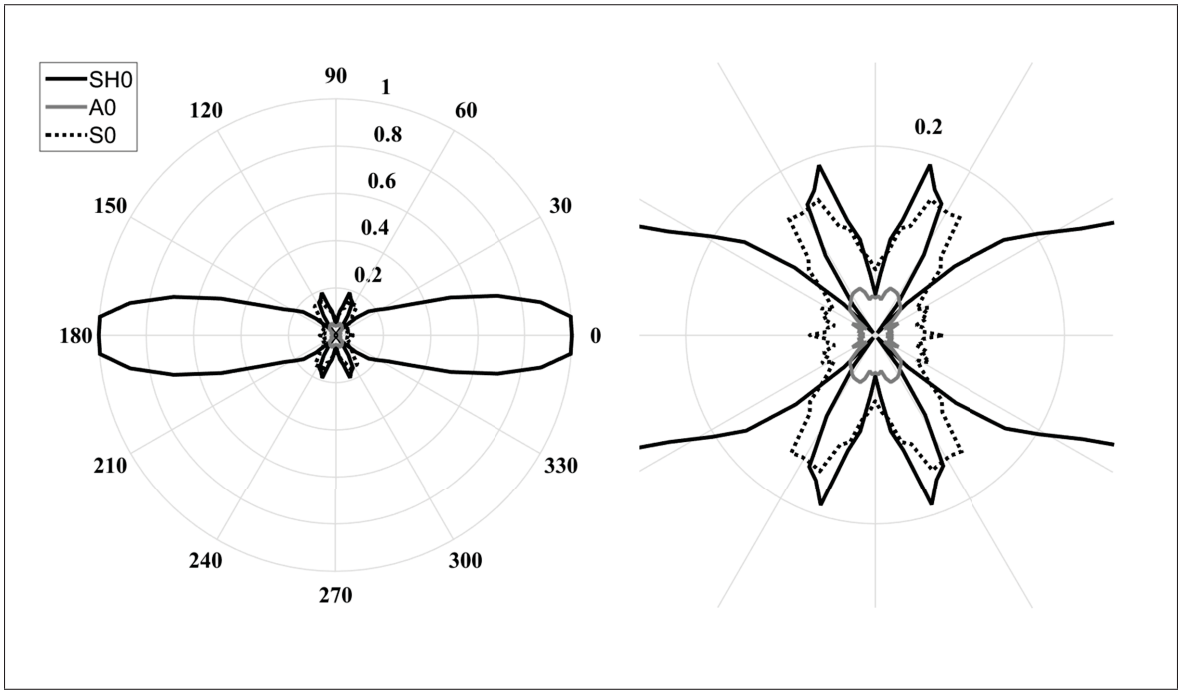

Figure 2.9 (a) Experimental directivity pattern of the fundamental obtained for a 3.7 mm wide transducer with an excitation centred at 425 kHz. The solid black lines represent the SH_0 mode, the dashed black lines represent the S_0 mode, and the solid light-grey lines represent the A_0 mode. (b) Four times zoom of the fundamental Lamb modes

As previously mentioned, the experimental validation was conducted for the PZT-5H rectangular plate geometry of 25.4 mm long, 3.7 mm wide, and 1 mm thick. The effect of the thickness is assumed to be negligible, as the thickness-shear resonant frequency is far away from the central excitation frequency of 425 kHz . The only effect in this range of frequencies is the attenuation due to the material properties, but it can be neglected for such hard and thin materials.

Samples were supplied with gold-plated electrodes already deposited, and the contacts and bonding for the validation were ensured using silver loaded epoxy (Chemtronics Conductive Epoxy). Five-cycle Hann-windowed toneburst centred at 425 kHz was used, as in the simula-

tions. The 3D component displacement along the same spatial line patterns at different angles was obtained using a Polytec PSV-500-3D-M laser Doppler scanning vibrometer. The same procedure was then used to obtain the transducer directivity pattern for all three modes according to their wavenumbers. Figure 2.9 illustrates the obtained experimental directivity patterns. The experimental results appear to agree very well with both simulation results. In fact, S_0 had an even lower amplitude in its propagation direction than in both simulations and the A_0 wave field had the expected shape and was, as expected from the simulations, at a very low amplitude. The desired SH_0 wave field appears to have the same aperture as predicted using both simulations but with a more constant amplitude at shallow angles.

Table 2.1 Ratio of maximum amplitude of both Lamb modes compared to the maximum amplitude of the SH_0 mode for all four design geometries for both simulation types and for the 425 kHz design for the experimental validation

	A_0/SH_0 (dB)	**S_0/SH_0 (dB)**
Analytical 213 kHz	-20.7	-9.2
Analytical 425 kHz	-26.2	-18.0
Analytical 631 kHz	-27.9	-21.5
Analytical 829 kHz	-29.5	-22.8
FEM 213 kHz	-11.9	-4.2
FEM 425 kHz	-19.6	-14.6
FEM 631 kHz	-24.5	-17.2
FEM 829 kHz	-16.4	-19.9
Experimental 425 kHz	-25.7	-16.4

Table 1 presents the ratio of amplitude in decibels of the Lamb modes compared to the SH_0 mode for all the design frequencies for both simulation types and the ratio for the experimental validation of the 425 kHz case.

2.6 Conclusion

This paper presented a geometric optimization procedure in order to develop a low-frequency piezo-ceramic transducer that is optimized to generate a plane SH_0 wave and to minimize the generation of the fundamental Lamb modes. The proposed procedure is for applications where the transducers are directly bonded to the structure but could be extended to other applications. Study of piezo-ceramics and different vibrational modes led to the choice of PZT-5H as an optimal material for the transducer design. Geometry of the piezoelectric sample has first been theoretically optimized and was then validated both with simulations and experimentally. It has been shown that, only by choosing the geometric parameters of a rectangular transducer wisely, it is possible to generate a directive SH_0 mode with an amplitude of, at least, 16.4 dB above both fundamental Lamb modes in any directions and of 23.0 dB above fundamental Lamb modes within an aperture of 20° for an optimized geometry corresponding to a central frequency of 425 kHz.

2.7 References

Alleyne, D., B. Pavlakovic, M. Lowe, and P. Cawley. 2004. "Rapid, long range inspection of chemical plant pipework using guided waves". In *Key Engineering Materials*. p. 434-441. Trans Tech Publ.

Belanger, P. 2009. "Feasibility of thickness mapping using ultrasonic guided waves". PhD thesis, Imperial College London.

Belanger, P. 2013. "High order shear horizontal modes for minimum remnant thickness". *Ultrasonics*, vol. 54, p. 1078-1087.

Buchanan, J. P. 1956. "Handbook of Piezoelectric Crystals for Radio Equipment Designers". *Philco Corporation*.

Cawley, P., M. Lowe, D. Alleyne, B. Pavlakovic, and P. Wilcox. 2003. "Practical long range guided wave testing: Applications to pipes and rail". *Material evaluation*, vol. 61 (1), p. 66-75.

Cheeke, J. D. N. 2012. "Fundamentals and Applications of Ultrasonic Waves, Second Edition". *CRC Press*.

Croxford, A., P. Wilcox, B. Drinkwater, and G. Konstantinidis. 2007. "Strategies for guided-wave structural health monitoring". In *Proceedings of the Royal Society of London A: Mathematical, Physical and Engineering Sciences*. p. 2961-2981. The Royal Society.

Dieulesaint, E. and D. Royer. 1999. "Ondes élastiques dans les solides. Tome 2, Génération, intéraction acousto-optique et applications". *Elsevier Masson*.

Drodz, M., L. Moreau, M. Castaings, M. J. S. Lowe, and P. Cawley. 2006. "Efficient Numerical Modelling of Absorbing Regions for Boundaries Of Guided Waves Problems". In *Quantitative Nondestructive Evaluation*. p. 126-133. AIP.

Hiroa, M. and H. Ogi. 1999. "An SH-wave EMAT technique for gas pipeline inspection". *NDT & E International*, vol. 32 (3), p. 127-132.

Jensen, J. A. 2002. "Imaging of Complex Media with Acoustic and Seismic Waves". *Topics in Applied Physics*, vol. 84, p. 135-166.

Mohamed, R. and P. Masson. 2010. "A time domain spectral element model for piezoelectric excitation of Lamb waves in isotropic plates". In *Health Monitoring of Structural and Biological Systems*. p. 76502G-1 - 76502G-11. SPIE.

Monkhouse, R., P. Wilcox, and P. Cawley. 1997. "Flexible interdigital PVDF transducers for the generation of lamb waves in structures". *Ultrasonics*, vol. 35, p. 489-498.

Nye, J. F. 1957. "Physical Properties of Crystals – Their Representation by Tensors and Matrices". *Oxford Science Publications*.

Ostiguy, P. C., N. Quaegebeur, K. R. Mulligan, P. Masson, and S. Elkoun. 2012. "In situ mechanical characterization of isotropic structures using guided wave propagation". *Smart Materials and Structures*, vol. 21 (6), p. 065010.

Pavlakovic, B., M. Lowe, D. Alleyne, and P. Cawley. 1997. "DISPERSE: A general purpose program for creating dispersion curves". In *Review of Progress in Quantitative NDE*. (San Diego, CA, USA 1997), p. 185-192. AIP.

Raghavan, A. and C. E. Cesnik. 2007. "Review of guided-wave structural health monitoring". *Shock and Vibration Digest*, vol. 39 (2), p. 91-114.

Ribichini, R., F. Cegla, P. B. Nagy, and P. Cawley. 2011. "Study and comparison of different EMAT configurations for SH wave inspection". *IEEE Transactions on Ultrasonics, Ferroelectrics and Frequency Control*, vol. 58 (12), p. 2571-2581.

Rose, J. 1999. "Ultrasonic Waves in Solid Media". *Cambridge Univeristy Press*.

Staszewski, C., G. Boller, and R. Tomlinson. 2004. "Health monitoring of aerospace structures: smart sensor technologies and signal processing". *John Wiley & Sons*.

Wilcox, P. D., P. Cawley, and M. J. S. Lowe. 1998. "Acoustic fields from PVDF interdigital transducers". In *Science, Measurements and Technology, IEE Proceedings*. p. 250-259.

CONCLUSION AND RECOMMENDATIONS

The aim of this masters thesis was to develop a piezo-ceramic acoustic transducer optimized for the generation of the fundamental SH guided wave mode suited for SHM applications. The focus of this work was not only on the maximization of the generated SH_0 mode but also on the minimization of the unfortunately generated fundamental Lamb modes, A_0 and S_0, in order to obtained the highest level of purity of the SH_0 mode. Such an approach was missing in the literature (discussed in Chapter 1).

The chosen approach was to optimize the classical design process of an acoustic transducer for shear strain generation for SHM applications. The first step was to choose the best suited material for such an endeavour and then to optimize the geometry of the transducer to maximize the SH_0 purity. The first chapter of this thesis presented the theoretical background that was required to fully achieve the goal. In addition, the fundamentals were discussed, detailed when required, and excellent textbooks were referred to the reader when details were not required. The first chapter also included an exhaustive review of the literature. In this section, every previously developed method used for the generation of SH waves is fully discussed and is also analyzed with regards to this project's motivation.

As this masters thesis is presented in the form of a thesis by publication, the second chapter was the originally submitted paper for publication in the journal *Ultrasonics*. In this chapter, the entire methodology was presented as well as both simulation type results and the experimentally validated results.

In the end, the chosen material was PZT-5H, a ceramic, as its d_{15} piezoelectric constant is relatively high and it is the only non-zero d_{1i} constant leading to the use of the shear-thickness mode of deformation. The rectangular geometry of the piezoelectric element in the proposed design methodology was chosen so that the width corresponds to half of the SH_0 wavelength

and, in a perfect situation, that the length corresponds to an integer multiple of both Lamb modes, which is a situation that appears very hard to obtain.

The second chapter also discussed the simulations that were conducted in order to validate the design assumptions. In the first simulation, an analytical simulation was carried out and the results were then validated using finite-element simulations, which is a more computer intensive solution. Finally, an experimental validation of the chosen design geometry was carried out. The results thus obtained, for the first time, with both simulation types, led to the choice of the ideal geometric parameters of the transducer out of the four previously determined optimal geometric sets. The chosen parameters were based on the central frequency of the transducer, 425 kHz, and are $L = 25.4$ mm, corresponding to exactly two times the S_0 wavelength, $w = 3.7$ mm, corresponding to half the wavelength of SH_0, and $t = 1$ mm. The thickness was discussed in Chapter 2 as having very little effect on the propagation of the SH modes.

The final results show that it is possible to generate the SH_0 mode at a level of purity of a minimum of 15 dB over both fundamental Lamb modes in any direction. Moreover, the proposed geometry allows the generation of a plane wave with a level of purity of 23 dB within an aperture of 20° in its propagation direction. Following these results, such a simple transducer design seems to be an interesting avenue in the future design of SHM systems for its low manufacturing cost, high level of purity, and flexibility of its optimized frequency.

Further work on the long-time reliability of such a solution in normal, as well as extreme, conditions, such as high temperature, would be relevant. To do so, the study of the bonding material would also be of great interest in further work, as it is a crucial factor in energy transmission for ultrasound. The extension of such a work to NDT applications would also be of great interest, and would require a complete classical transducer design, including wear plate and backing mass, which would have to be optimized for the SH_0 wave generation.

APPENDIX I

ARTICLE: DEVELOPMENT OF A LOW-FREQUENCY PIEZO-CERAMIC TRANSDUCER FOR THE GENERATION OF PLANE SHEAR HORIZONTAL GUIDED WAVES

Guillaume Boivin[1], Martin Viens[1], Pierre Belanger[1]

[1] Département de Génie Mécanique, École de Technologie Supérieure,
1100 Notre-Dame Ouest, Montréal, Québec, Canada H3C 1K3

This article was published in the « QNDE 2015 » proceedings in February 2016

1. Abstract

The shear horizontal guided wave fundamental mode (SH0) has the particularity of being the only non-dispersive plate guided wave mode. This characteristic makes this ultrasonic guided wave mode very attractive in non-destructive testing, facilitating signal processing for long range inspections. It is, however, difficult to generate only a single guided wave mode when using piezoelectric transduction. This work aims to develop a piezoelectric transducer capable of generating a virtually pure plane zeroth order shear horizontal wave. The chosen material was the PZT-5H for its dominant d15 piezoelectric constant, which makes it a perfect candidate for SH-wave generation. The transducer dimensions were optimised using an analytical model based on the Huygens' principle of superposition and the dipole pattern of a shear point source. A 3D multiphysics finite element model was then used to validate the analytical model results. Experimental validation was finally conducted with a laser Doppler vibrometer (LDV) system. Excellent agreement between the analytical model, finite element model and experimental validation was seen.

2. Introduction

Guided ultrasonic waves are now routinely used in non-destructive testing (NDT) and structural health monitoring (SHM) because they can propagate over long distances, making the screening of large areas faster and reducing the number of ultrasonic transducers necessary to

achieve inspections. Unfortunately, an important characteristic of guided waves is that they are dispersive. The only non-dispersive mode is the fundamental Shear Horizontal mode, commonly called SH_0. The non-dispersive aspect of the fundamental SH mode, combined with its low attenuation due to fluid loading, makes it particularly attractive. Given the nature of the displacement components composing SH waves, out-of-plane stress is absolutely necessary to generate it, and will unfortunately also generate both Lamb modes types. In fact, an in-plane displacement will generate SH waves perpendicular to the excitation direction, but will also generate all Lamb modes that can exist at the frequency of excitation in the direction parallel to the excitation. Several methods have been studied in the past in order to generate SH waves. Among them, the EMAT (Electro Magnetic Acoustic Transducer) is a well-documented solution, but it requires a high power source, it is very sensitive to misalignment, and it is too bulky of a solution to make it interesting for aerospace SHM applications (Ma *et al.* (2014)). Interdigital PVDF (Wilcox *et al.* (1998)) is yet another known solution for generating or receiving SH modes. Unfortunately, because of its low piezoelectric coefficients, it requires a lot of fingers to generate high amplitudes, which makes it hard to reduce the size of the transducer. Piezoceramics have long been used for conventional UT, and recently, for the generation and detection of guided waves. Unfortunately, very few documented examples using piezoceramics to generate or detect SH waves exist in the literature (Zhou *et al.* (2015) and Kamal and Giurgiutiu (2014)), and none of them seems to focus on the selectivity of SH modes. This paper discusses the development of a low frequency piezoelectric transducer for the generation of plane SH0 waves with high mode purity. The first section discusses the design assumptions, including the selection of the material and the optimization of the geometry. The second section discusses numerical simulations, first analytically, and then using FE models, in order to characterize the directivity of the transducer and to validate the geometric design assumptions. Finally, the third and last section presents the experimental validation.

3. Design Assumptions

The first step in developing a transducer that is optimized to generate a SH_0 wave is understanding the excitation mechanism. Shear horizontal waves are shear-guided waves, but unlike

the Lamb wave modes, they propagate perpendicular to the direction of excitation. Using the coordinate system in Fig. 1, a y-axis harmonic point source excitation will act as a dipole, meaning that SH modes will propagate cylindrically in both x-axis directions, and that Lamb modes will propagate cylindrically in both y-axis directions, as illustrated in Fig. 1.

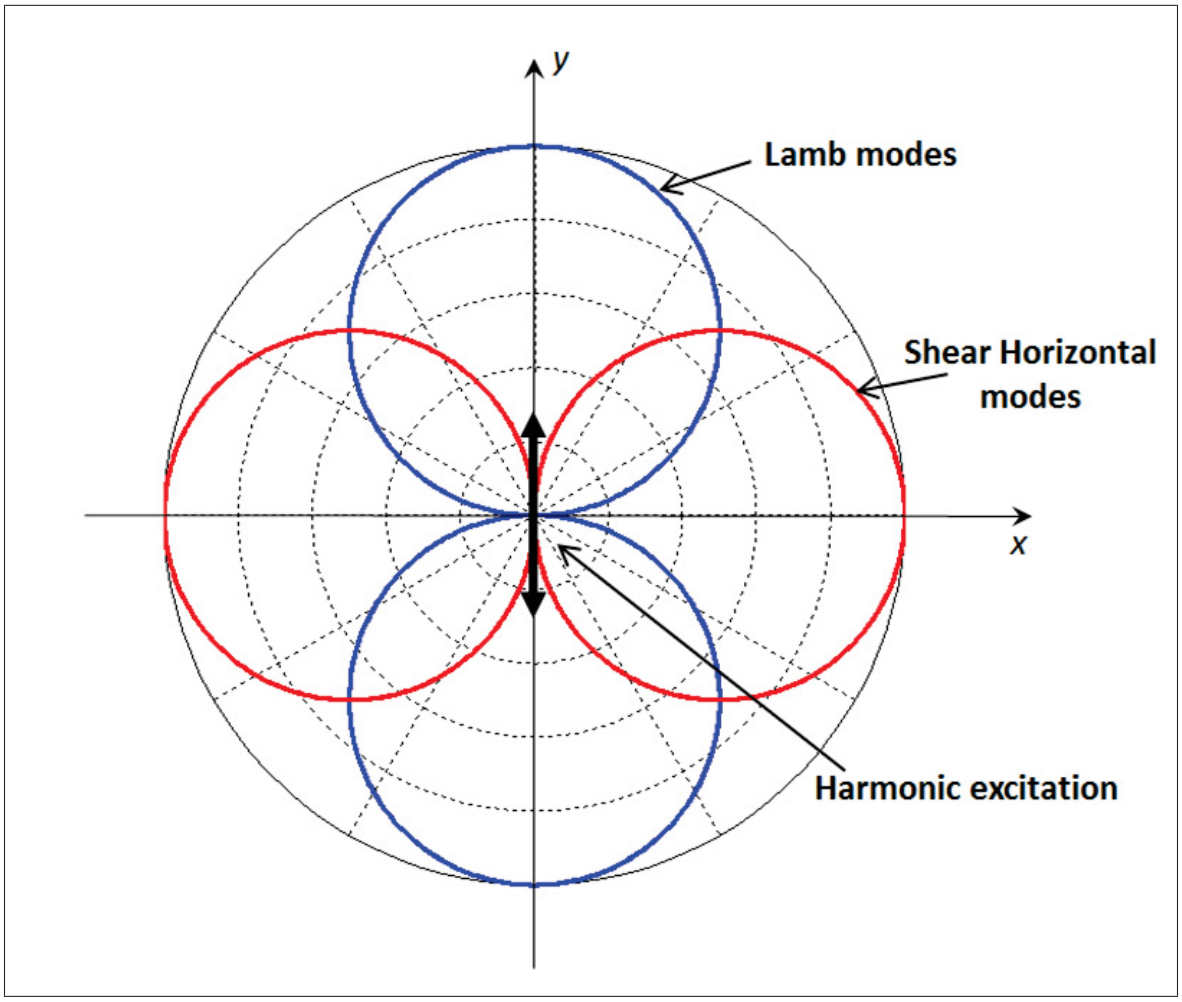

Figure-A I-1 Dipole directivity pattern of Lamb and shear horizontal modes due to a harmonic surface shear stress point source excitation

3.1 Material Selection

The chosen material must provide the possibility of inducing a significant shear stress to the substrate. The category of piezoceramics called the PZT (Lead Zirconate Titanate) has been selected because it is very well documented in the literature for conventional UT applications and its commercial availability. The chosen material was the PZT-5H, being the one that presents the greatest d_{15} piezoelectric coupling coefficient among all soft and hard materials in the PZT family, and also because its piezoelectric coupling matrix, like for all the PZTs, has only one non-null coefficient in its first row, which is the d15. For this particular reason, if the PZT sample is poled in the right direction, always referred to as the 3^{rd} axis, and the electrodes are placed across the 1st axis, applying a voltage will result in a pure torsional moment around the 2^{nd} axis without any other undesired displacement component. The piezoelectric coupling coefficient matrix of the PZT-5H is shown in Table 1.

Table-A I-1 PZT-5H piezoelectric coupling coefficients (Berlincourt *et al.* (2003))

	$\mathbf{d}_{31}$	$\mathbf{d}_{33}$	$\mathbf{d}_{15}$
PZT-5H coefficients (x 10-12 m/V)	-274	593	741

3.2 Geometry Optimization

The basic starting geometry used in order to generate a plane directional SH wave was chosen to be a simple rectangle poled in the length, which referred to as the 3^{rd} piezoelectric conventional axis, with the parameters L being the length, w the width, and t the thickness, as shown in Fig. 2. The width was first fixed at the half of the wavelength of the desired SH_0 central frequency in order to maximize the sum of the energy under the transduction surface over each cycle. The central frequency was arbitrarily chosen to be at 400 kHz, leading to a width (w) of 3.9 mm. The frequency was chosen to ensure that only all three fundamental modes can be excited, even with a very broadband excitation, and SH1 cutoff frequency being 985 kHz in a 1.5875 mm thick plate.

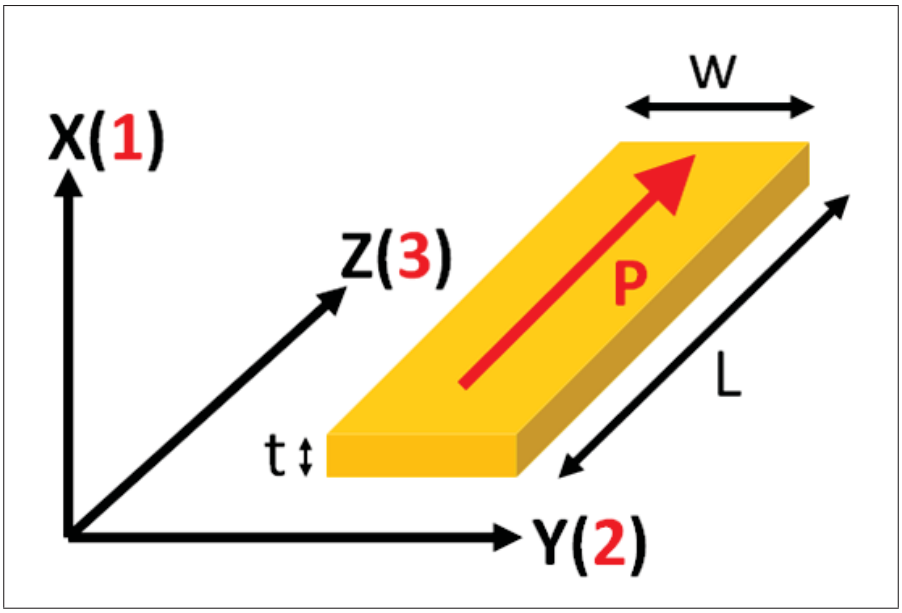

Figure-A I-2 PZT-5H sample geometric parameters, poling direction with top and bottom electrodes

The length was chosen to be 25.4 mm (1 inch) as it was the manufacturing upper limit. Moreover, it is theoretically proven that at the exact size of the wavelength or less, a source will act as a source point, as shown in Fig. 1 (Jensen (2002)). Therefore, in order to focus the aperture of the directivity pattern of the generated modes, the relative transduction size of each generated mode, L, for the SH_0 mode, and w for both A_0 and S_0 modes, has to be minimally greater than its proper wavelength. Table 1 presents the according ratio showing that, unfortunately, the S_0 and A_0 beams may act like dipoles due to their ratio of less than one, which should lead to a significant aperture.

Table-A I-2 Ratio of relative transduction size to wavelength for each fundamental mode

Fundamental mode	**A_0 (w/λ_{A0})**	**S_0 (w/λ_{S0})**	**SH_0 (L/λ_{SH_0})**
Ratio of relative size to wavelength	0.7610	0.2887	3.2460

As the width was fixed to the desired SH_0 half wavelength in order to maximize the excitation, the relationship between the length and the Lamb modes wavelength is the same, as shown in

Table 2; if the length is close to an odd multiple of the half wavelength, it will maximize the amplitude of the mode at a 0° angle, according to the propagation direction of this particular mode (two lobes will exist at ±45°, but will be of lower amplitude). Conversely, if the length is close to an even multiple of the half wavelength, it will have the same effect, but instead of maximizing the amplitude at a 0° angle according to the propagation direction, it will minimize it with the two low amplitude lobes at ±45° still subsisting.

Knowing this relationship, the goal would be to have the ratio of the length L to the wavelength as close as possible to an integer in order to minimize the amplitudes of the Lamb modes. Table 3 shows that the A0 mode should practically be zero at 0° and that S_0 should be small.

Table-A I-3 Ratio of relative transduction depth to wavelength for each fundamental mode

Fundamental mode	**A_0 (L/λ_{A0})**	**S_0 (L/λ_{S0})**	**SH_0 (w/λ_{SH_0})**
Ratio of relative size to wavelength	4.9561	1.8801	0.4984

Finally, Table 4 presents the chosen geometric dimensions of the PZT-5H sample.

Table-A I-4 Geometric dimension of the sample

Dimension	**L**	**t**	**w**
Value	25.4 mm	1 mm	3.9 mm

4. Numerical Simulations

Two different types of wave propagation simulations were used in order to properly characterize the transducer with the previously defined parameters – analytical simulation and ABAQUS FE simulation. Since FE 3D wave propagation simulations are considerably computer-intensive, the analytical model which neglects the physical interaction between the plate and the transducer was initially implemented to validate the design assumptions. The input signal was chosen to be a 5-cycles Hann windowed toneburst centered at 400 kHz, and this signal was

used for every simulation presented in this review and for the experimental validation when the time domain was used.

4.1 Analytical Model

First, an analytical wave propagation model combining the Huygens' superposition principle and the dipole pattern of a source point as presented in Fig. 1 was implemented to validate the directivity pattern of the PZT sample. This model simulates the propagation over the interface between the plate and the transducer, assuming a uniform displacement field across the entire surface. The first step was to simulate the displacement field over a distance r, an angle theta and for a time range using (Wilcox *et al.* (1998)):

$$u(r,\theta,t) = \frac{sin(\theta)}{2\pi}\sum_{m}\int_{-\infty}^{+\infty} A(\omega)E_m(\omega)H_0^{(1)}(k(\omega)r)e^{i\omega t}d\omega \qquad \text{(A I-1)}$$

where A(ω) is the complex amplitude of excitation, E_m is the in-plane excitability of the mth mode, $H_0{}^1$ is the Hankel function of the first kind, and the term sin(θ) is the dipole directivity of the SH mode (this term changes to cos(θ) for the Lamb modes). The second step was to discretized the transduction surface in a series of source points, with a minimum of 4 source points per wavelength, to ensure convergence (Kamal and Giurgiutiu (2014)) and to sum the acoustic field of every discretized point source over the transduction surface, and to then observe the resulting acoustic field at the desired frequency, distance and time.

4.2 FE Simulations

Finite element simulations were conducted using the explicit package of the commercial software, ABAQUS. A full 3D model was used, even though it is very computer-intensive, in order to propagate both Lamb and SH modes at the same time (Belanger (2013)) without neglecting physical interactions between the plate and the transducer.

Since the explicit ABAQUS package does not allow the use of piezoelectric elements, implicit

package simulations were used to extract the real displacement field, which was then used as the input for the time domain simulations. The complete model, including the plate and the transducer, were simulated using an 8-nodes C3D8R element. The plate was assumed to be isotropic, and the PZT to be orthotropic. The size of the elements was chosen to be of a tenth of the smallest propagating wavelength (Drodz *et al.* (2006)) to ensure proper wave propagation. Table 5 presents the different simulation parameters that were used. The time increment was chosen to be less than the element size divided by the greatest wave velocity for the same reason.

Table-A I-5 Geometric dimension of the sample

Parameter	**Element size**	**Time increment**	**Plate length (square)**	**Plate thickness**
Value	0.5 mm	50 ns	304 mm	1.5875 mm

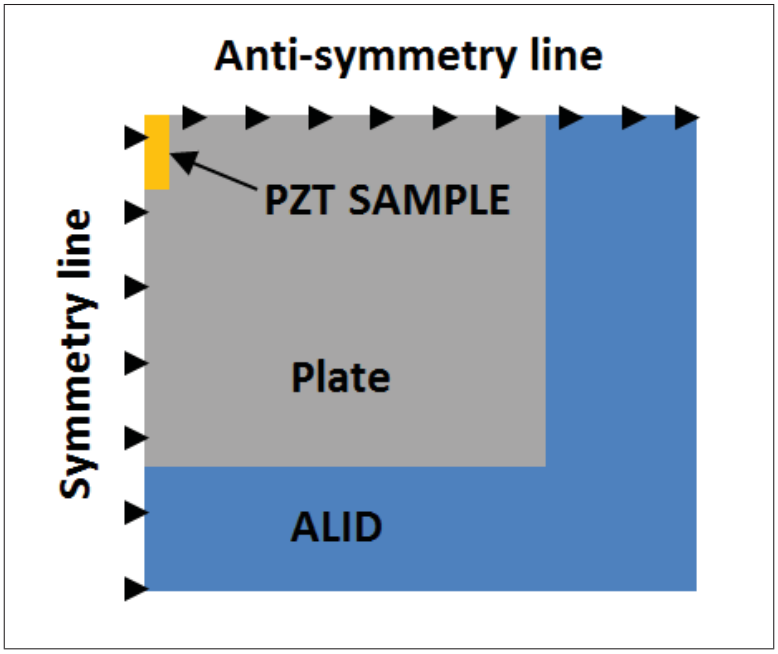

Figure-A I-3 Schematic of the FE reduced model used to propagate both Lamb and SH modes

ALID boundaries were used to reduce the model size and to avoid reflections from the edges of the plates [8]. The piezoceramics plate was positioned in the middle of a plate, and two axis of

symmetry were used to reduce computational time, one symmetry in the SH_0 mode propagation direction and one anti-symmetry in the Lamb modes propagation direction, as shown in Fig. 3. The plate simulated was made of aluminum, with a Young's modulus of 69 GPa, a Poisson ratio of 0.33 and a density of 2700 g/cm^3.

4.3 Simulation Results

For the analytical model, the data was extracted at a precise distance of 300mm over a quarter of a circle arc, and the time at which every mode amplitude was extracted was the time at which the amplitude was at its maximum. For the FE models, angular lines of output were extracted on a quarter of a circle arc allowing a spatial FFT to be performed on each of the radial lines in order to separate each propagating and reflected modes by its wavenumber. Directivities were then built using the maximum of each wavenumber at every extracted angle. Figure 4 shows the directivity pattern obtained for both simulation types with the previously determined geometric parameters of the transducer.

The results from the FE model present the same directivity pattern as the one obtained with the analytical model, except for the S0 beam, which presents a smaller aperture than expected, but which is also of approximately the same maximum amplitude. As geometrically predicted, in both cases, the A0 mode directivity presents small amplitudes and an aperture close to a point source. Both modes present a ratio of amplitude to the SH_0 mode amplitude of a minimum of -30dB at an aperture of ±10° around the desired direction of propagation of SH_0 mode in the FE result.

5. Experimental Validation

For the experimental validation, gold-plated electrodes were deposited on the bottom and top surfaces of the PZT-5H sample. The PZT was then bonded to the middle of an aluminum plate using silver loaded epoxy to ensure electrical contact between the plate and the bottom electrode. A wire was then glued to the top electrode using the same epoxy.

The displacement field over the plate was extracted using a 3D scanning LDV (Laser Doppler

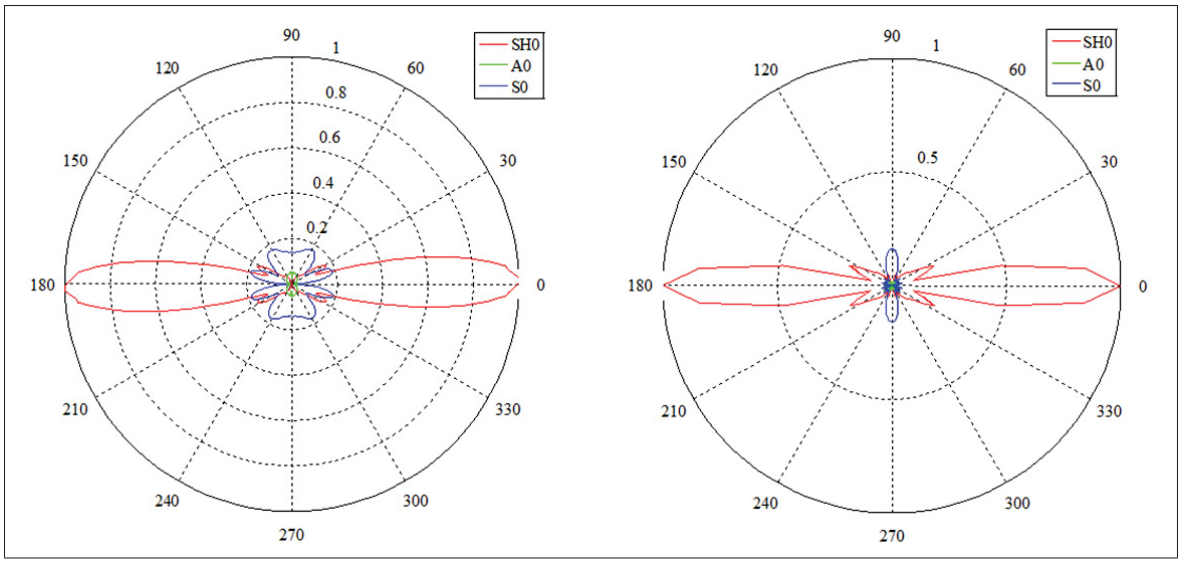

Figure-A I-4 Directivity pattern of a) the analytical model, and b) the FE model

Vibrometer) system from Polytec (PSV-500-3D). The same pattern as for the FE model was extracted in order to obtain the wavenumber amplitude at every angle and to trace the directivity pattern. Reflective paint was sprayed all over the region of interest to ensure diffusion of the laser beam. A pseudo-random excitation signal was used to obtain a large frequency bandwidth response, and because the SNR (signal-to-noise ratio) is greater in the frequency domain than in the time domain for this type of equipment. Acoustic absorbent material was used at the boundaries of the plate to avoid reflections allowing the performance of such a steady state analysis with this type of excitation. Fig. 5 shows the LDV system from Polytec, as well as the experimental setup.

Because frequency domain acquisition was performed and because of the nature of the analysis that is performed by the LDV system, which is a stationary analysis, absorbent material had to be applied on every edge of the plate to avoid reflections. Otherwise it would become impossible to differentiate the different reflections and the incident signal even using spatial FFT.

The directivity pattern obtained from the experimental measurements are presented in Fig. 6 a) and Fig. 6 b) (at a 16-times magnification) to observe the S_0 directivity lobes precisely. These

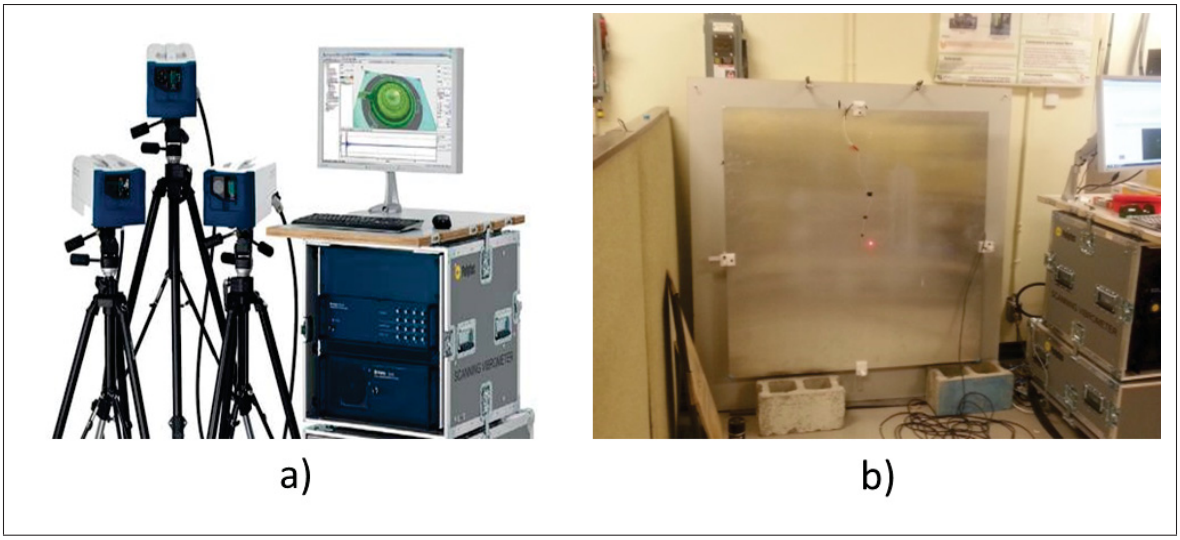

Figure-A I-5 a) Polytec PSV-500-3D, b) Experimental validation setup

beams present expected features, but also non-null amplitudes values at a 0° angle, which is unexpected as it contradicts what was previously observed in both simulations results. Many reasons might explain these non-null components, including a non-uniform sample (polycrystalline) polarization, a non-uniform physical bonding, and misalignment of the sample, which could all result in residual misaligned in-plane displacement, explaining S_0 amplitudes at low angles.

Except for the higher amplitude values at low angle, which still appear to be at a minimum of 20 dB below the SH_0 mode at an aperture of ±10° around the direction of propagation, the results obtained experimentally agree very well with both models in terms of general trends and amplitude. The aperture of the S_0 mode around its main propagation direction tends to be more similar to that obtained with the analytical model than does the one with the FE model, but the difference is small.

6. Conclusion

Geometric optimization to obtain an SH_0 piezoelectric transducer has been presented theoretically, and then validated both with simulations and experimentally. It has been shown that only

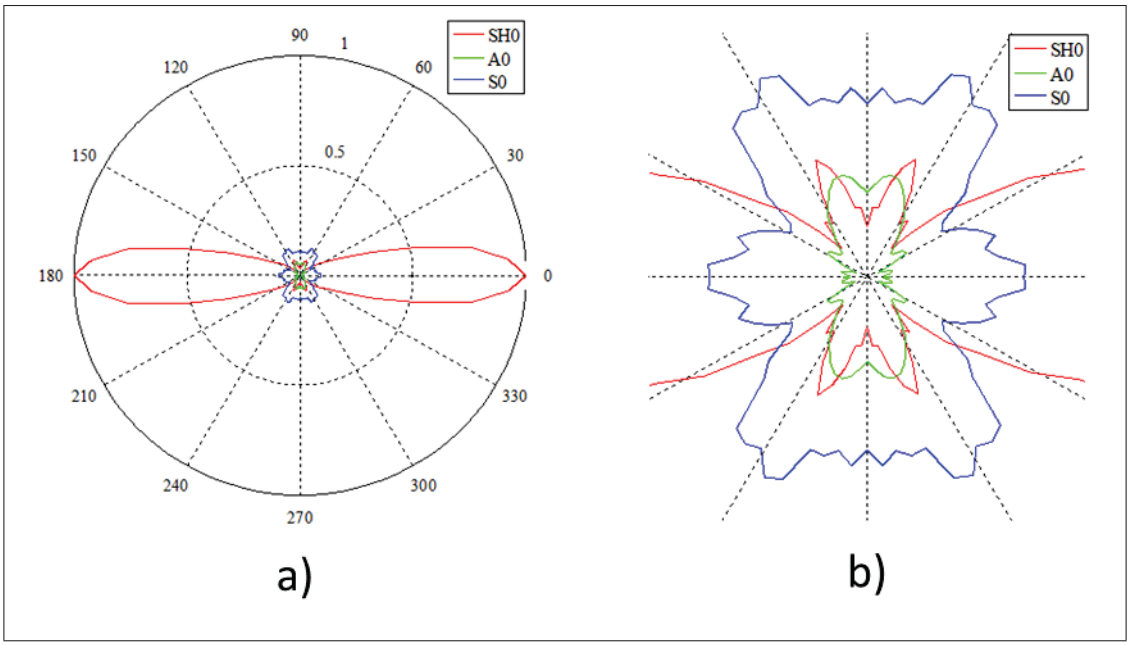

Figure-A I-6 a) Experimental directivity pattern of the PZT sample b) Experimental directivity pattern 16x centered zoom

by choosing the geometric parameters of a rectangular transducer wisely can it be possible to generate a directive SH_0 mode of amplitude at a minimum of 20 dB over Lamb modes over an aperture of 20°; we also see that the maximum amplitude of undesired Lamb modes that propagates at an angle of 90° compared to the maximum amplitude of the SH_0 mode, at 0°, is 17.6 dB lower.

7. Acknowledgments

The work was supported by the Consortium for Research and Innovation in Aerospace in Québec (CRIAQ), including Bombardier Aerospace, L-3 MAS, NRC, CTA, McGill University and Université de Sherbrooke as part of the CRIAQ DPHM-501 project.

8. References

Belanger, P. 2013. "High order shear horizontal modes for minimum remnant thickness". *Ultrasonics*, vol. 54, p. 1078-1087.

Berlincourt, D., H. H. A. Krueger, and C. Near. 2003. "Technical Publication TP-226 Properties of Piezoelectricity Ceramics". *Morgan Electro Ceramics*.

Drodz, M., L. Moreau, M. Castaings, M. J. S. Lowe, and P. Cawley. 2006. "Efficient Numerical Modelling of Absorbing Regions for Boundaries Of Guided Waves Problems". In *Quantitative Nondestructive Evaluation*. p. 126-133. AIP.

Jensen, J. A. 2002. "Imaging of Complex Media with Acoustic and Seismic Waves". *Topics in Applied Physics*, vol. 84, p. 135-166.

Kamal, A. and V. Giurgiutiu. 2014. "Shear horizontal wave excitation and reception with shear horizontal piezoelectric wafer active sensor (SH-PWAS)". *Smart Materials and Structures*, vol. 23, p. 085019.

Ma, Q., J. Jiao, P. Hu, X. Zhong, B. Wu, and C. He. 2014. "Excitation and detection of shear horizontal waves with electromagnetic acoustic transducers for nondestructive testing of plates". *Chinese Journal of Mechanical Engineering*, vol. 27, p. 428-436.

Wilcox, P. D., P. Cawley, and M. J. S. Lowe. 1998. "Acoustic fields from PVDF interdigital transducers". In *Science, Measurements and Technology, IEE Proceedings*. p. 250-259.

Zhou, W., H. Li, and F. G. Yuan. 2015. "Fundamental understanding of wave generation and reception using d36 type piezoelectric transducers". *Ultrasonics*, vol. 57, p. 135-143.

BIBLIOGRAPHY

Alleyne, D., B. Pavlakovic, M. Lowe, and P. Cawley. 2004. "Rapid, long range inspection of chemical plant pipework using guided waves". In *Key Engineering Materials*. p. 434-441. Trans Tech Publ.

Balageas, D., C.-P. Fritzen, and A. Güemes. 2006. "Structural Health Monitoring". *Wiley*.

Belanger, P. 2009. "Feasibility of thickness mapping using ultrasonic guided waves". PhD thesis, Imperial College London.

Belanger, P. 2013. "High order shear horizontal modes for minimum remnant thickness". *Ultrasonics*, vol. 54, p. 1078-1087.

Böttger, W., H. Schneider, and W. Weingarten. 1987. "Prototype EMAT System for Tube Inspection with Guided Ultrasonic Waves". *Nuclear Engineering and Design*, vol. 102, p. 369-376.

Buchanan, J. P. 1956. "Handbook of Piezoelectric Crystals for Radio Equipment Designers". *Philco Corporation*.

Cartz, L. 1995. "Nondestructive Testing: Radiography, Ultrasonics, Liquid Penetrant, Magnetic Particle, Eddy Current". *ASM International*.

Cawley, P. and D. Alleyne. 1996. "The use of Lamb waves for the long range inspection of large structure". *Ultrasonics*, vol. 34, p. 287-290.

Cawley, P., M. Lowe, D. Alleyne, B. Pavlakovic, and P. Wilcox. 2003. "Practical long range guided wave testing: Applications to pipes and rail". *Material evaluation*, vol. 61 (1), p. 66-75.

Cheeke, J. D. N. 2012. "Fundamentals and Applications of Ultrasonic Waves, Second Edition". *CRC Press*.

Clarke, T., F. Simonetti, S. Rohklin, and P. Cawley. 2009. "Development of a Low-Frequency High Purity A0 Mode Transducer for SHM Applications". *IEEE Transactions on Ultrasonics, Ferroelectrics and Frequency Control*, vol. 56, p. 1457-1468.

Croxford, A., P. Wilcox, B. Drinkwater, and G. Konstantinidis. 2007. "Strategies for guided-wave structural health monitoring". In *Proceedings of the Royal Society of London A: Mathematical, Physical and Engineering Sciences*. p. 2961-2981. The Royal Society.

Demma, A., P. Cawley, and M. Lowe. 2003. "Scattering of the fundamental shear horizontal mode from steps and notches in plates". *The Journal of the Acoustical Society of America*, vol. 113, p. 1880-1891.

Dieulesaint, E. and D. Royer. 1999. "Ondes élastiques dans les solides. Tome 2, Génération, interaction acousto-optique et applications". *Elsevier Masson*.

Drodz, M., L. Moreau, M. Castaings, M. J. S. Lowe, and P. Cawley. 2006. "Efficient Numerical Modelling of Absorbing Regions for Boundaries Of Guided Waves Problems". In *Quantitative Nondestructive Evaluation*. p. 126-133. AIP.

Fortunko, C. M., R. B. King, and M. Tan. 1982. "Nondestructive evaluation of planar defects in plates using low frequency shear horizontal waves". *Journal of Applied Physics*, vol. 53, p. 3450.

Graff, K. F. 1991. "Wave Motion in Elastic Solids". *Dover Publications inc.*

Hiroa, M. and H. Ogi. 1999. "An SH-wave EMAT technique for gas pipeline inspection". *NDT & E International*, vol. 32 (3), p. 127-132.

Jaffe, B., W. R. Cook Jr, and H. Jaffe. 1971. "Piezoelectric Ceramics, Non-Metallic Solids: A Series of Monographs, Number 3". *Academic Press London and New York*.

Jensen, J. A. 2002. "Imaging of Complex Media with Acoustic and Seismic Waves". *Topics in Applied Physics*, vol. 84, p. 135-166.

Kamal, A. and V. Giurgiutiu. 2014. "Shear horizontal wave excitation and reception with shear horizontal piezoelectric wafer active sensor (SH-PWAS)". *Smart Materials and Structures*, vol. 23, p. 085019.

Krautkrämer, J. and H. Krautkrämer. 1990. "Ultrasonic Testing of Materials, 4th, fully revised Edition". *Springer-Verlag*.

Lamb, H. 1917. "On waves in an elastic plate". In *Proceedings of the Royal Society of London*. p. 114-128.

Leinov, E., M. J. S. Lowe, and P. Cawley. 2015. "Investigation of guided wave propagation and attenuation in pipe buried in sand". *Journal of Sound and Vibration*, vol. 347, p. 96-114.

Mohamed, R. and P. Masson. 2010. "A time domain spectral element model for piezoelectric excitation of Lamb waves in isotropic plates". In *Health Monitoring of Structural and Biological Systems*. p. 76502G-1 - 76502G-11. SPIE.

Monkhouse, R., P. Wilcox, and P. Cawley. 1997. "Flexible interdigital PVDF transducers for the generation of lamb waves in structures". *Ultrasonics*, vol. 35, p. 489-498.

Nye, J. F. 1957. "Physical Properties of Crystals – Their Representation by Tensors and Matrices". *Oxford Science Publications*.

Ostiguy, P. C., N. Quaegebeur, K. R. Mulligan, P. Masson, and S. Elkoun. 2012. "In situ mechanical characterization of isotropic structures using guided wave propagation". *Smart Materials and Structures*, vol. 21 (6), p. 065010.

Pavlakovic, B., M. Lowe, D. Alleyne, and P. Cawley. 1997. "DISPERSE: A general purpose program for creating dispersion curves". In *Review of Progress in Quantitative NDE*. (San Diego, CA, USA 1997), p. 185-192. AIP.

Qingzeng, M., J. Jingpin, H. Ping, Z. Xi, W. Bin, and H. Cunfu. 2014. "Excitation and Detection of Shear Horizontal Waves with Electromagnetic Acoustic Transducers for Nondestructive Testing of Plates". *Chinese Journal of Mechanical Engineering*, vol. 27, p. 428-436.

Raghavan, A. and C. E. Cesnik. 2007. "Review of guided-wave structural health monitoring". *Shock and Vibration Digest*, vol. 39 (2), p. 91-114.

Rajagopal, P. and M. Lowe. 2007. "Short range scattering of the fundamental shear horizontal guided wave mode normally incident at a through-thickness crack in an isotropic plate". *The Journal of the Acoustical Society of America*, vol. 122 (3), p. 1527-1538.

Ratassepp, M., M. J. S. Lowe, P. Cawley, and A. Klausson. 2008. "Scattering of the fundamental shear horizontal mode in a plate when incident at a through crack aligned in the propagation direction of the mode". *The Journal of the Acoustical Society of America*, vol. 124, p. 2873-2882.

Ribichini, R., F. Cegla, P. B. Nagy, and P. Cawley. 2011. "Study and comparison of different EMAT configurations for SH wave inspection". *IEEE Transactions on Ultrasonics, Ferroelectrics and Frequency Control*, vol. 58 (12), p. 2571-2581.

Rose, J. 1999. "Ultrasonic Waves in Solid Media". *Cambridge Univeristy Press*.

Staszewski, C., G. Boller, and R. Tomlinson. 2004. "Health monitoring of aerospace structures: smart sensor technologies and signal processing". *John Wiley & Sons*.

Thompson, R. B., G. A. Alers, and M. A. Tennison. 1972. "Application of Direct Electromagnetic Lamb Wave Generation to Gas Pipeline Inspection". In *1972 Ultrasonics Symposium*.

Wilcox, P., M. Lowe, and P. Cawley. 2000. "Lamb and SH Wave Transducer Arrays for the Inspection of Large Areas of Thick Plates". In *Proceedings of the 15th World Conference on Nondestructive Testing*.

Wilcox, P., M. Evans, B. Pavlakovic, D. Alleyne, K. Vine, P. Cawley, and M. Lowe. 2003. "Guided wave testing of rail". *Insight-Non-Destructive Testing and Condition Monitoring*, vol. 45, n° 6, p. 413-420.

Wilcox, P., M. Lowe, and P. Cawley. 2005. "Omnidirectional Guided Wave Inspection of Large Metallic Plate Structure Using an EMAT Array". *IEEE Transactions on Ultrasonics, Ferroelectrics and Frequency Control*, vol. 52, p. 653-665.

Wilcox, P. D., P. Cawley, and M. J. S. Lowe. 1998. "Acoustic fields from PVDF interdigital transducers". In *Science, Measurements and Technology, IEE Proceedings*. p. 250-259.

Zhou, W., H. Li, and F. G. Yuan. 2015. "Fundamental understanding of wave generation and reception using d36 type piezoelectric transducers". *Ultrasonics*, vol. 57, p. 135-143.